Mice carrying nonsense mutant p53 develop frequent multicentric or metastatic tumors

Running title: High tumor and metastases rate in *Trp53*^{R210X} mice

Charlotte Strandgren[1,2], Veronica Rondahl[2], Ann-Sophie Oppelt[1], Susanne Öhlin[1], Angelos Heldin[1], and Klas G. Wiman[1*]

[1]Karolinska Institutet, Dept. of Oncology-Pathology, Stockholm, Sweden

[2]Swedish University of Agricultural Sciences, Dept. of Animal Biosciences, Uppsala, Sweden

*Corresponding author: Klas Wiman; email: Klas.Wiman@ki.se

Conflict of interest

KGW is co-founder and shareholder of Aprea Therapeutics, a company that develops novel cancer therapy by targeting the DNA damage response pathway. KGW has previously received salary and research funding from Aprea Therapeutics. KGW is board member of the company MyCural Therapeutics AB. The other authors declare no conflicts of interest.

Abstract

The *TP53* tumor suppressor gene is mutated in a large fraction of human tumors. Close to 11% of *TP53* mutations are nonsense mutations, causing premature termination of protein synthesis and expression of truncated inactive p53 protein. The most common *TP53* nonsense mutation in human cancer is R213X. To study the impact of *TP53* nonsense mutations *in vivo*, we generated mice harboring the *Trp53* nonsense mutation R210X that corresponds to human *TP53*-R213X. Initially, *Trp53*^{R210X} mice appear phenotypically normal, although the proportion of female *Trp53*$^{R210X/R210X}$ mice is dramatically reduced. Female homozygous mice are poor breeders and remain smaller and lighter than female heterozygous and wildtype littermates. *Trp53*$^{R210X/R210X}$ mice start to show tumors at 2.5 months of age, and their maximal lifespan is 8.5 months. *Trp53*$^{R210X/+}$ mice present tumors from 9 months of age, and by 16.5 months of age 50% of all heterozygous mice have developed overt tumors. 71% of tumors from *Trp53*$^{R210X/+}$ mice show loss of heterozygosity (LOH). Homozygous mice develop hematopoietic and mesenchymal tumors, most commonly T-cell lymphoma and leiomyosarcoma, and heterozygous mice develop hematopoietic, mesenchymal, epithelial and sex cord tumors, most commonly osteosarcoma and leiomyosarcoma. The tumor phenotype is similar to that of *Trp53-null* and *Trp53*-missense knock-in mice, although the *Trp53*$^{R210X/R210X}$ mice have a high rate of multicentric or metastatic tumors, and *Trp53*$^{R210X/+}$ mice have a longer overall survival than *Trp53*$^{R172H/+}$ missense mutant knock-in mice. Treatment of T-cell lymphoma cells from *Trp53*$^{R210X/R210X}$ mice with aminoglycoside G418 induces expression of full-length functional p53 and apoptotic cell death. Our new unique mouse model will allow further studies of the effects of *Trp53* nonsense mutation in a multi-organ system and serve as a model for the Li-Fraumeni syndrome (LFS). It will also be valuable for preclinical

evaluation of novel therapeutic strategies for targeting *TP53* nonsense mutations in cancer.

Introduction

The transcription factor p53 is activated by cellular stress (1). Activated p53 binds to specific DNA motifs as a tetramer, transactivates multiple target genes (2, 3), and controls multiple processes, including cell cycle progression, DNA repair, metabolism, senescence, and apoptosis (1, 4). The *TP53* gene is often inactivated in human tumors, most frequently by missense mutations that disrupt p53 DNA binding and transactivation of target genes (5, 6). Missense mutant p53 can inhibit co-expressed wildtype (WT) p53 through a dominant-negative effect that can increase resistance to genotoxic stress and drive clonal selection (7). Some forms of missense mutant p53 may exert oncogenic gain-of-function (GOF) activity, associated with a wider tumor spectrum and enhanced invasion and metastasis (8-10). However, other studies have not found evidence for mutant p53 GOF activity (7, 11, 12) and it is likely that mutant p53 GOF depends on cell background. For instance, myeloid malignancies may behave differently than solid tumors (7). A recent detailed characterization of *TP53* variants in HCT116 cells demonstrated R175H mutant p53 GOF only after long-term *in vitro* passaging, associated with increased mutant p53 levels and manifested as enhanced migration, invasion and metastasis (13). Around 11% of *TP53* mutations are nonsense mutations that result in a premature stop codon (6) and expression of truncated p53 that lacks critical functional domains and therefore fails to transactivate p53 target genes. Nevertheless, certain truncated p53 proteins generated by *TP53* nonsense mutations may have oncogenic properties (14).

72 Mouse models that either completely lack p53 or carry missense mutant p53 (*Trp53*^{Mis})
73 support a key role of p53 as tumor suppressor. Homozygous *Trp53*-null or *Trp53*^{Mis}
74 mice show a striking cancer phenotype with a high rate of spontaneous tumors and
75 reduced survival compared to WT mice (9, 15-20). Both *Trp53*$^{-/-}$ and *Trp53*$^{Mis/Mis}$ mice
76 exhibit tumors from 3-6 months of age, whereas *Trp53*$^{+/-}$ and *Trp53*$^{Mis/+}$ mice display
77 tumors at 9-10 months of age, often associated with loss of the WT allele (loss of
78 heterozygosity, LOH). *Trp53*$^{-/-}$ and *Trp53*$^{Mis/Mis}$ mice mainly develop lymphomas and
79 sarcomas, whereas heterozygotes, especially the *Trp53*$^{Mis/+}$ models, also develop
80 carcinomas. *Trp53*$^{R172H/+}$ and *Trp53*$^{R270H/+}$ mice develop more invasive and metastasis
81 prone tumors compared to *Trp53*$^{+/-}$ mice, consistent with GOF activity for these
82 mutants (9, 17). However, a mouse model of colorectal cancer with inactivated *Apc*
83 and activated *Kras* alleles did not show any significant difference between *Trp53*-null
84 and R270H mutant alleles in life span, adenocarcinoma incidence and metastasis (21).
85
86 Mouse models designed to investigate the functional implications of *TP53* nonsense
87 mutations *in vivo* have previously not been established. Such models are crucial for a
88 better understanding of the impact of nonsense mutant p53 in a living organism and
89 can also serve as platforms for preclinical development of pharmacological strategies
90 for therapeutic targeting of nonsense mutant *TP53* in cancer. Several compounds can
91 induce translational readthrough of nonsense mutant *TP53* and thus expression of full-
92 length and functional p53 protein in cultured cells, including G418 (22), Clitocine (23),
93 ELX-02 (24), 2,6-Diaminopurine (25), cc-90009 (26), and 5-Fluorouridine (27). Here
94 we present a novel mouse model carrying the *Trp53*-R210X nonsense mutation that
95 corresponds to *TP53*-R213X, the most common *TP53* nonsense mutation in human
96 tumors (6).

97

98 # Results

99 **Generation of a *Trp53*^{R210X} mouse model**

100 To generate a mouse model harboring the *Trp53*-R210X nonsense mutation, we used
101 CRISPR/Cas9 genome editing to introduce two single point mutations resulting in an
102 Arg (CGC) to STOP (TGA) substitution at codon 210 in exon 6 (Fig. 1A). The
103 CRISPR/Cas9 strategy was validated in NIH/3T3 mouse fibroblasts. Single-cell clones
104 of edited NIH/3T3 cells were genotyped as heterozygous using the introduced XbaI
105 cleavage site. PCR amplicons of *Trp53* exons 5-7 from the NIH/3T3 cell clones were
106 subcloned and sequencing of individual plasmid clones identified those carrying the
107 R210X mutation and the two downstream silent mutations. However, the XbaI site was
108 not present in all clones (Fig. 1B). ssODN template-triggered repair can generate short
109 conversion tracts of about 30 nucleotides with Gaussian-like distributions surrounding
110 the Cas9 cut site (28). The mutation producing the intended XbaI site was too far from
111 the Cas9 cut site and therefore outside of the effective conversion zone, explaining its
112 inconsistent introduction.

113

114 Genotyping the F0 offspring with PCR revealed that 6/17 pups were positive for the
115 R210X mutation. Sanger sequencing confirmed that two of the six pups also had the
116 XbaI site, whereas the remaining four lacked it (not shown). The pups were also
117 genotyped with restriction enzyme digestion, which confirmed the two pups carrying
118 the XbaI site, and also identified one pup carrying the XbaI site but not the correctly
119 mutated R210X sequence. The six F0 offspring carrying the correct R210X mutation
120 were set up for backcross breeding to WT C57BL/6J mice to eliminate possible off-
121 target events. Two founder animals, both lacking the XbaI site, generated F1 offspring,

122 and PCR genotyping verified germline transmission of the R210X allele (Fig. 1C).
123 Sequencing of 1049 bp surrounding the edited *Trp53* exon 6 locus confirmed clean
124 WT and R210X alleles in all F1 mice identified as heterozygous (Fig. 1D).
125
126 **Intercrosses of *Trp53*^{R210X} mice yield fewer and smaller female homozygous**
127 **offspring**
128 The *Trp53*^{R210X} strain was maintained by backcrossing *Trp53*$^{R210X/+}$ mice to WT
129 C57BL/6J mice. Backcross litter sizes at 2 weeks of age were normal compared to the
130 reference litter size of 7.0 pups for C57BL/6J mice (*informatics.jax.org*)
131 (Supplementary Table S1), and genotype and sex distribution (309 offspring) was
132 consistent with expected Mendelian inheritance but with significantly more WT males
133 (Supplementary Table S2). Different combinations of intercrosses were set up to
134 assess the viability and reproductive capacity of *Trp53*$^{R210X/R210X}$ mice (Supplementary
135 Table S1). Intercrossing only *Trp53*$^{R210X/R210X}$ mice resulted in litters with significantly
136 fewer pups at 2 weeks of age compared to backcrosses, whilst intercrosses with at
137 least one *Trp53*$^{R210X/+}$ mouse yielded similar litter sizes as the backcrosses
138 (Supplementary Table S1; Supplementary Fig. S1). Among the 13 intercrosses
139 between *Trp53*$^{R210X/R210X}$ and *Trp53*$^{R210X/+}$ mice, only one litter was derived using a
140 *Trp53*$^{R210X/R210X}$ female, yielding a single male *Trp53*$^{R210X/+}$ pup. All other 12 litters were
141 spawned from *Trp53*$^{R210X/+}$ females. Thus, *Trp53*$^{R210X/R210X}$ female mice are fertile but
142 have a reduced breeding capacity.
143
144 Intercrosses between *Trp53*$^{R210X/+}$ and/or *Trp53*$^{R210X/R210X}$ mice gave fewer female
145 *Trp53*$^{R210X/R210X}$ offspring (Supplementary Table S2), whereas male offspring
146 distribution followed expected Mendelian inheritance regardless of genotype. Females

147 remained fewer when all *Trp53*$^{R210X/R210X}$ offspring were analyzed. Aside from the poor
148 breeding capacity of female *Trp53*$^{R210X/R210X}$ mice, heterozygous and homozygous
149 mice of both genders appeared phenotypically normal at young age and were fertile.
150
151 *Trp53*^{R210X} mouse bodyweights were recorded weekly from postnatal week 2 and until
152 euthanasia for all offspring from homozygous-generating intercrosses. Female
153 *Trp53*$^{R210X/R210X}$ mice had smaller body size (not shown) and were lighter than both WT
154 and *Trp53*$^{R210X/+}$ littermates at 2 weeks of age and remained lighter throughout life (Fig.
155 2A). In contrast, male mice had almost identical weight development regardless of
156 genotype until 34 weeks of age, when the remaining *Trp53*$^{R210X/R210X}$ males were
157 markedly lighter than their *Trp53*$^{R210X/+}$ and WT littermates, most likely due to
158 emaciation secondary to tumor growth (Fig. 2B).
159
160 ***Trp53*^{R210X} mice have a reduced lifespan**
161 The *Trp53*$^{R210X/R210X}$ mice had significantly shorter survival than *Trp53*$^{R210X/+}$ and WT
162 mice (adj. P-values: ***$p < 0.001$), as did *Trp53*$^{R210X/+}$ mice compared to WT (adj. P-
163 value: ***$p < 0.001$) (Fig. 2C-E). Female and male *Trp53*$^{R210X/R210X}$ mice had similar
164 survival, whilst female *Trp53*$^{R210X/+}$ mice had reduced survival compared to male (p =
165 0.003) (Fig. 2F). Male WT mice showed a significantly shorter mean survival compared
166 to female WT mice (p = 0.043), which may be related to the fact that 11 male WT mice
167 <1.5 years old were found dead or were euthanized due to wounds or abdominal
168 masses. Only one of these had abdominal neoplasia; all others either showed no gross
169 abnormalities or had enlarged seminal vesicles, a normal phenomenon in aging male
170 mice (29).
171

172 We also compared *Trp53*$^{R210X/R210X}$ survival to that of *Trp53*$^{R172H/R172H}$ missense knock-
173 in mice maintained in the same animal facility. Survival of both mouse strains showed
174 a similar rapid decline from 3-8.5 months of age, and their mean survival showed no
175 statistically significant difference: 145.5 days for *Trp53*$^{R210X/R210X}$ mice and 155 days
176 for *Trp53*$^{R172H/R172H}$ mice (Fig. 2C-E). In contrast, *Trp53*$^{R210X/+}$ mice survived
177 significantly longer than *Trp53*$^{R172H/+}$ mice (adj. P-value: $p = 0.01$), with a mean survival
178 of 492 days vs. 469 days (Fig. 2E). There were no differences in survival between
179 female and male *Trp53*^{R172H} mice (Fig. 2G).
180

181 **Tumor development in *Trp53*^{R210X} mice is highly penetrant**

182 All animals, both euthanized and found dead, were necropsied, and histopathological
183 analysis was performed on available tissues from all *Trp53*$^{R210X/R210X}$ mice and a subset
184 of *Trp53*$^{R210X/+}$ and WT mice. Grossly visible tumors were found in 59 of 62 (95%)
185 *Trp53*$^{R210X/R210X}$ mice, 152 of 209 (73%) *Trp53*$^{R210X/+}$ mice, and 30 of 66 (45%) WT
186 mice. This confirms a highly penetrant tumor phenotype in *Trp53*^{R210X} mice.
187 Histopathological examination was performed on tissues from 49 *Trp53*$^{R210X/R210X}$ mice
188 (those with formalin-fixed tissues available) and 79 (those with formalin-fixed tissues
189 available) of the 85 *Trp53*$^{R210X/+}$ mice with suspected tumors that were randomly
190 selected for LOH analysis (see below). To identify a baseline for common tumors in
191 the WT parents and siblings of the *Trp53*^{R210X} mutant mice, we also examined tumors
192 and tissues from the oldest of the available necropsied WT mice (12 males, 12
193 females). Among the analyzed mice, 48 (98%) of the *Trp53*$^{R210X/R210X}$ mice and 79
194 (100%) of the *Trp53*$^{R210X/+}$ mice had histopathologically diagnosable tumors. Twenty
195 (83%) of the selected WT mice had tumors and were thus considered a good
196 representation of the background tumor panorama (Supplementary Table S3).

197

198 **Different tumor spectra in *Trp53*$^{R210X/R210X}$ and *Trp53*$^{R210X/+}$ mice**

199 *Trp53*$^{R210X/R210X}$ mice only developed hematopoietic tumors and soft-tissue
200 mesenchymal tumors (Fig. 3; Supplementary Fig. S2A-C; Supplementary Table S4A),
201 whereas *Trp53*$^{R210X/+}$ mice showed a broader tumor spectrum with hard-tissue
202 mesenchymal tumors, soft-tissue mesenchymal tumors, hematopoietic tumors,
203 epithelial tumors, and a single sex cord tumor (Fig. 4A-D; Supplementary Fig. S3A-C;
204 Supplementary Table S4B), which included both malignant and benign tumors
205 (Supplementary Table S3). WT mice had a broad spectrum of both malignant and
206 benign tumors (Supplementary Table S4C; Supplementary Fig. S4A-C). Malignant
207 tumors were classified as solitary when they were found in a single organ or tissue,
208 hematopoietic tumors found in at least two organs or tissues were classified as
209 multicentric, and mesenchymal and epithelial tumors found in at least two organs and
210 tissues were classified as metastatic. To assess loss of the WT *Trp53* allele (LOH) in
211 tumors from *Trp53*$^{R210X/+}$ mice, we performed semi-quantitative PCR with the primers
212 for genotyping (Fig. 4E). Out of 132 tumors analyzed from *Trp53*$^{R210X/+}$ mice, 94 (71%)
213 showed LOH, consistent with a strong selection pressure to eliminate the remaining
214 WT allele.

215

216 T-cell lymphomas, confirmed by positive CD3 staining, were only found in homozygous
217 (66.7 %) and heterozygous (5.1 %) mice (Fig. 5A; Supplementary Fig. S2A-B, S3A;
218 Supplementary Table S4A-D). Only *Trp53*$^{R210X/R210X}$ mice had solitary thymic T-cell
219 lymphoma, but the most common type of lymphoma in homozygous mice was
220 multicentric thymic T-cell lymphoma, which was less common in *Trp53*$^{R210X/+}$ mice and
221 absent in WT mice (Fig. 5B; Supplementary Table S4A-C). In *Trp53*$^{R210X/+}$ and in WT

222 mice the most common type of lymphoma was multicentric pleomorphic lymphoma.
223 Pleomorphic lymphomas, confirmed by immunohistochemistry (IHC) (Supplementary
224 Table S4A-C) were most frequent in WT mice and lowest in homozygous mice (adj. P-
225 value: $p = 0.0048$) (Fig. 5A).
226
227 Similarly, malignant soft-tissue sarcomas were only found in homozygous and
228 heterozygous mice (Fig. 5A and C; Supplementary Fig. S5A; Supplementary Table
229 S4A-C). Of the other mesenchymal tumor types, osteosarcoma was only found in
230 heterozygous mice (25.3 %), and both genotypes had similar proportions of soft-tissue
231 sarcomas (Fig. 5A and C; Supplementary Fig. S5A; Supplementary Table S4A-B).
232 *Trp53*$^{R210X/R210X}$ mice developed primary soft-tissue sarcomas in subcutis, skin, and
233 skeletal muscle (Fig. 3; Supplementary Fig. S2C; Supplementary Table S4A), whereas
234 *Trp53*$^{R210X/+}$ mice developed soft-tissue sarcomas in these sites as well as in numerous
235 other organs, including urogenitalia (Fig. 4; Supplementary Fig. S3B; Supplementary
236 Table S4B). The majority of soft-tissue sarcomas were myosarcomas – primarily
237 leiomyosarcomas that were confirmed by positive desmin staining and negative
238 myogenin staining, and rhabdomyosarcomas confirmed by positive desmin and
239 negative myogenin staining (Fig. 3 and 4; Supplementary Fig. S2C, S3B, S5A;
240 Supplementary Table S4A-B). Female *Trp53*$^{R210X/+}$ had more frequent osteosarcomas
241 than males (adj. P-value: $p = 0.0028$) (Fig. 5D). *Trp53*$^{R210X/R210X}$ and WT mice showed
242 no significant differences between sexes (Supplementary Fig. S5B-C).
243
244 To visualize the *in situ* distribution of lymphoma in a *Trp53*$^{R210X/R210X}$ mouse, we
245 performed post-mortem MRI on a 234-days old male that was euthanized due to a
246 large tumor on the ventral neck and respiratory distress. The MRI showed extensive

247 neoplasias originating and extending from the thymus and several lymph nodes (Fig.
248 5E-G).
249
250 **Frequent multicentric/metastatic tumors with variable impact on survival**
251 Nearly two-thirds of the *Trp53*$^{R210X/R210X}$ mice (29 of 48; 60%) had multicentric or
252 metastatic tumors (Supplementary Tables S3 and S4A). Of these, 25 were T-cell
253 lymphomas (of 32 T-cell lymphomas in total), three were other hematopoietic tumors,
254 and one a soft-tissue sarcoma. The most common lymphoma sites were thymus,
255 spleen, lung and liver, followed by kidney, heart, and submandibular salivary gland
256 (Fig. 3A-B; Supplementary Fig. S2A-B; Supplementary Table S4A). In comparison,
257 only a little more than one-third of the heterozygous mice (29 of 79; 37%) had
258 multicentric or metastatic tumors (Supplementary Tables S3 and S4B). Twenty-two
259 were hematopoietic tumors, three were soft-tissue sarcomas, three were
260 osteosarcomas, and one a carcinoma. Half of the tumor-bearing WT mice (10 of 20,
261 50%) had multicentric or metastatic tumors, and all these were hematopoietic tumors
262 (Supplementary Tables S3 and S4C). The number of organs and tissues with
263 neoplasia are probably underestimated, since not all tissues were sampled from all
264 animals.
265
266 There was no significant effect of multicentric or metastatic disease on survival of
267 *Trp53*$^{R210X/R210X}$ mice (p = 0.0595), whereas *Trp53*$^{R210X/+}$ mice with multicentric or
268 metastatic disease had significantly longer survival than mice with only solitary tumors
269 (p = 0.0167) (Fig. 6A). To elucidate if tumor type was prognostic of survival in mice
270 with solitary malignant tumors, we extracted survival data for the most common tumor
271 type in each genotype and compared to the remaining mice with solitary tumors. We

272 found no differences in survival between solitary T-cell lymphomas and other malignant
273 solitary tumors in homozygous mice, or between solitary osteosarcomas and other
274 malignant, solitary tumors in heterozygous mice (Fig. 6B). However, *Trp53*$^{R210X/R210X}$
275 mice with solitary T-cell lymphoma, but not *Trp53*$^{R210X/R210X}$ mice with solitary soft-
276 tissue sarcomas, had significantly shorter survival than mice with multicentric or
277 metastatic tumors (Fig. 6C). Furthermore, *Trp53*$^{R210X/R210X}$ mice with thymic lymphoma
278 showed decreased survival compared to those with both thymic and splenic lymphoma
279 (Fig. 6D). Since thymic tumors can interfere with heart and lung function, we also
280 investigated thymic tumor size. *Trp53*$^{R210X/R210X}$ mice with only thymic lymphoma had
281 the largest thymus tumors compared to mice with splenic lymphoma or both thymic
282 and splenic lymphoma (Fig. 6E).
283

284 **Translational readthrough in T-cell lymphoma cells derived from *Trp53*$^{R210X/R210X}$**
285 **mice**

286 To investigate if translational readthrough of R210X nonsense mutant *Trp53* can
287 generate full-length active p53, we established T-cell lymphoma lines from thymic
288 lymphomas of *Trp53*$^{R210X/R210X}$ mice (X405, X491 and X547). As controls, we used T-
289 cell lymphoma lines established from thymic lymphomas of *Trp53*$^{R172H/R172H}$ mice
290 (H661 and H671). Fig. 7A shows HE and CD3 IHC staining of thymus from mouse
291 X405, verifying T-cell origin of the tumor. Supplementary Fig. S6A shows
292 corresponding histological images for thymi of *Trp53*$^{R210X/R210X}$ mice X491 and X547
293 as well as *Trp53*$^{R172H/R172H}$ mice H661 and H671. All cell lines were analyzed with PCR
294 to confirm the correct genotype (Supplementary Fig. S6B). Flow cytometry with CD3,
295 CD4 and CD8 antibodies verified T-cell origin, with 97.5% $CD3^+$ cells and >99% among
296 those $CD4^+CD8^+$ (Fig. 7B). To examine translational readthrough, we treated T-cell

297 lymphoma cells with aminoglycoside G418 for 72 h. Immunofluorescence staining with
298 anti-p53 C-terminal antibody (280aa C-term) that detects full-length p53 but not C-
299 terminally truncated p53, and anti-p53 N-terminal antibody N1 that detects both full-
300 length and C-terminally truncated p53, showed that 100μM G418 induced full-length
301 p53 (Fig. 7C), and that treatment with 200μM G418 caused substantial cell death
302 (Supplementary Fig. S6C). Western blotting with anti-p53 antibody 1C12 that
303 recognizes an N-terminal epitope confirmed a dose-dependent induction of
304 translational readthrough and expression of full-length p53 (Fig. 7D; Supplementary
305 Fig. S7A). We also found a slight increase in truncated p53, most likely due to inhibition
306 of nonsense-mediated decay following translational readthrough (30). Moreover, qRT-
307 PCR revealed a dose-dependent upregulation of p53 target genes *Puma* and *Zmat3*
308 and to a lesser extent *Cdkn1a* (*p21*) and *Bax* in all *Trp53*$^{R210X/R210X}$ T-lymphoma cell
309 lines but not in T-lymphoma cell lines derived from *Trp53*$^{R172H/R172H}$ mice upon
310 treatment with G418 (Fig. 7E; Supplementary Fig. S7B), confirming that full-length p53
311 induced by G418 is functional as transcription factor. G418 also inhibited cell
312 proliferation in a dose-dependent manner in T-lymphoma cells derived from both
313 *Trp53*$^{R210X/R210X}$ and *Trp53*$^{R172H/R172H}$ mice as shown by the WST-1 assay, but with
314 significantly higher efficiency in the *Trp53*$^{R210X/R210X}$-derived T-lymphoma lines (Fig. 7F;
315 Supplementary Fig. S7C). Finally, G418 at 150 and 200μM induced apoptotic cell
316 death in the T-lymphoma cells as shown by Annexin V flow cytometry (Fig. 7G;
317 Supplementary Fig. S8). This cell death was significantly more efficient in the
318 *Trp53*$^{R210X/R210X}$ T-lymphoma cells than in the *Trp53*$^{R172H/R172H}$ T-lymphoma cells at
319 200μM G418.
320

321 **Discussion**

322 We present here the first mouse model carrying a *Trp53* nonsense mutation. *Trp53*-
323 R210X corresponds to human *TP53*-R213X, one of the 10 most common *TP53*
324 mutations in human tumors. The *Trp53*^{R210X} allele was transferred at Mendelian
325 frequency in all crosses except intercrosses with female *Trp53*$^{R210X/R210X}$ mice that
326 resulted in smaller litters than the reference number for the C57BL/6J WT background
327 strain. These results are consistent with data from *Trp53*-null mice, where significant
328 decreases in embryonic implantation, pregnancy rate and litter size were observed in
329 matings with female *Trp53*$^{-/-}$ mice (31). This effect in *Trp53*-null mice is most likely
330 caused by reduced levels of leukemia inhibitory factor (LIF), which may also be
331 pertinent to our new *Trp53*^{R210X} strain.
332
333 We observed a substantial reduction in the frequency of female *Trp53*$^{R210X/R210X}$ pups
334 regardless of breeding setup, consistent with previous data for *Trp53*-null mice (32-
335 35). Exencephaly and craniofacial malformations in *Trp53*$^{-/-}$ female embryos (32, 33,
336 35) may also explain the skewed gender distribution observed in the *Trp53*$^{R210X/R210X}$
337 mice. Apart from the poor breeding capacity of female *Trp53*$^{R210X/R210X}$ mice,
338 heterozygous and homozygous mice of both genders appeared phenotypically normal
339 initially and were fertile, as reported for *Trp53*-null mice (15, 16).
340
341 The reduced bodyweights of female *Trp53*$^{R210X/R210X}$ mice compared to *Trp53*$^{R210X/+}$
342 and WT mice was unexpected. To our knowledge, similar findings have not been
343 reported for any genetically manipulated *Trp53*-model; in one study, female and male
344 *Trp53*$^{+/-}$ and *Trp53*$^{-/-}$ mice showed no difference in bodyweight (34), and two recently
345 published *Trp53* missense knock-in mouse models displayed normal male and female
346 bodyweights (19). In our study, male mice of all three genotypes had almost identical

347 weight curves up until 34 weeks of age, very similar to those reported for male *Trp53*-
348 null mice (34). At that point, the weight curve for male *Trp53*$^{R210X/R210X}$ mice began to
349 deviate downward from those of *Trp53*$^{R210X/+}$ and WT mice, presumably a direct
350 consequence of tumor development.
351
352 *Trp53*$^{R210X/R210X}$ mice had similar survival curves as the control *Trp53*$^{R172H/R172H}$ mice,
353 as well as several other published *Trp53*-null and *Trp*53^{Mis} mouse models (9, 15-20,
354 34). Interestingly, *Trp53*$^{R210X/+}$ mice showed significantly longer survival than the
355 *Trp53*$^{R172H/+}$ mice in our colony. One plausible explanation for this difference is that the
356 truncated p53 protein encoded by the *Trp53*^{R210X} allele exerts a less pronounced
357 dominant-negative effect by oligomerization with co-expressed WT p53 as compared
358 to R172H missense mutant p53, or completely lacks such effect, allowing more potent
359 WT p53-dependent tumor suppression in *Trp53*$^{R210X/+}$ mice.
360
361 As reported for homozygous *Trp53*-null and *Trp53* missense knock-in mice (9, 15-20),
362 homozygous *Trp53*^{R210X} mice showed a remarkable susceptibility to tumor
363 development at an early age, with lymphoma as the predominant tumor type, (79.2%
364 in *Trp53*$^{R210X/R210X}$ mice and 57-78% in homozygous *Trp53*-null and *Trp53*^{Mis} mice)
365 followed by soft-tissue sarcoma (35.4% in *Trp53*$^{R210X/R210X}$ mice and 22-38% in
366 homozygous *Trp53*-null and *Trp53*^{Mis} mice). This confirms that *Trp53* nonsense
367 mutation at codon 210 leads to a dramatically increased tumor incidence, just like
368 complete loss or missense mutation of *Trp53*. The most common lymphoma type in
369 *Trp53*$^{R210X/R210X}$ mice was T-cell lymphoma (84% of lymphoma cases). T-cell
370 lymphomas and soft-tissue sarcomas can be considered as *de novo* tumor types, since
371 they were never found in the WT mice, and are very rare in the background C57BL6/J

372 strain (36). In contrast, pleomorphic lymphoma and histiocytic sarcoma, which were
373 found in 20.8% of the homozygous mice, are common tumor types that are found at
374 all ages, although at increasing incidence with age, and cannot therefore be reliably
375 associated with the homozygous genotype (37, 38).
376
377 Whereas all homozygous *Trp53*^{R210X} mice had died or been euthanized by 8.5 months
378 of age, heterozygosity for the *Trp53*^{R210X} mutation did not begin to affect survival until
379 approximately 9 months of age. Like homozygous *Trp53*^{R210X} mice, heterozygous mice
380 showed a striking tumor phenotype, although with larger variation in tumor type and
381 later onset of clinical signs compared to homozygous mice, and with frequent LOH,
382 again in agreement with previous studies of *Trp53*-null and *Trp53* missense knock-in
383 mouse models (9, 15-17, 20, 39). Heterozygous mice also developed the *de novo* soft-
384 tissue sarcomas, and more rarely T-cell lymphoma, as well as osteosarcomas,
385 mammary gland carcinomas, and in one case a malignant Leydig cell tumor, none of
386 which are reported as a spontaneous tumor in C57BL/6J mice (36, 40). The malignant
387 Leydig cell tumor is of particular interest since its presence shows that this mouse
388 model also can develop tumors of sex cord origin, i.e. testicular or ovarian, in addition
389 to the more frequent hematopoietic, mesenchymal and epithelial tumors. Thus, the
390 *Trp53*$^{R210X/+}$ mice, like previously published *Trp53*-null and missense knock-in models,
391 represent a valuable model for the Li-Fraumeni syndrome (LFS), in which *TP53*
392 nonsense mutations occur with a similar frequency as in somatic tumors according to
393 The *TP53* Database collection of germline variants (The *TP53* Database (R21, Jan
394 2025): https://tp53.cancer.gov) (41). The delayed tumor onset in *Trp53*$^{R210X/+}$
395 compared to *Trp53*$^{R210X/R210X}$ mice reflects the need to eliminate the remaining WT

396 allele. This provides time for acquisition of additional genetic alterations that might
397 predispose to other tumor types than those reported in C57BL/6J mice (36, 40).
398
399 *Trp53*$^{R210X/R210X}$ mice frequently developed multicentric lymphomas, most commonly
400 with tumors in liver and lung, and one leiomyosarcoma metastasis, whereas the
401 *Trp53*$^{R210X/+}$ mice showed a comparatively lower rate of multicentric lymphoma and
402 higher rate of soft-tissue sarcoma metastasis. Unexpectedly, multicentric or metastatic
403 disease did not have a negative effect on survival of *Trp53*^{R210X} mice. However, it
404 should be noted that solitary tumors without metastasis can be life-threatening through
405 various mechanisms, such as rapid growth that compromises organ function, e.g.
406 compression and restriction of heart and lungs by thymic lymphomas, or production of
407 substances that affect vital organs or have detrimental systemic effects.
408
409 The observed high rate of lymphoma multicentricity in *Trp53*^{R210X} mice is in contrast to
410 data for *Trp53*$^{R246S/R246S}$, *Trp53*$^{R245W/R245W}$ and *Trp53*$^{R270H/R270H}$ mice that only
411 infrequently or never develop multicentric or metastatic disease (18, 20). This could
412 suggest that truncated p53 derived from the R210X nonsense mutant allele can exert
413 some kind of GOF activity. Indeed, GOF features of C-terminally truncated p53
414 proteins have been demonstrated in cell culture and *in vivo* assays (14). However, we
415 did not observe any significant differences in overall survival, tumor incidence, tumor
416 spectrum or LOH frequency between our *Trp53*^{R210X} mice and data reported for *Trp53*-
417 null mice (15, 16, 39), arguing against a prominent GOF activity of the R210X allele in
418 this setting. A caveat is that specific data on multicentricity or metastasis frequency in
419 homozygous *Trp53*-null or missense knock-in mice are limited in previous studies (9,

420 15-20). Thus, we do not exclude that further investigation will reveal GOF properties
421 of nonsense mutant *TP53*.
422
423 To validate the utility of our model as a platform for the development of nonsense
424 mutant *TP53*-targeted anti-cancer drugs, we showed that the well-known readthrough
425 inducer G418 could restore expression of full-length and functional p53 in T-lymphoma
426 cell lines derived from *Trp53*$^{R210X/R210X}$ mice. We observed upregulation of p53 target
427 genes in the T-lymphoma cell lines derived from *Trp53*$^{R210X/R210X}$ mice but not in
428 *Trp53*$^{R172H/R172H}$ T-lymphoma control cell lines. The observation that G418 inhibited cell
429 growth and induced apoptotic cell death with statistically significant higher efficiency in
430 the *Trp53*$^{R210X/R210X}$ lymphoma cells than in the *Trp53*$^{R172H/R172H}$ lymphoma cells
431 confirms a p53-dependent biological effect, although G418 also has p53-independent
432 general toxicity.
433
434 In conclusion, our *Trp*53^{R210X} mouse model should facilitate the development of novel
435 strategies for therapeutic targeting of nonsense mutant *TP53* in cancer. Importantly,
436 we have demonstrated that induction of translational readthrough of the *Trp53*-R210X
437 allele in mouse thymic lymphoma cells results in the expression of full-length and
438 functional p53 protein and cell death by apoptosis. Further studies of downstream
439 effects of p53 activation in these cells are required, and it will also be interesting to
440 examine translational readthrough and p53 activation in cell lines derived from other
441 types of tumors in *Trp53*^{R210X} mice. Induction of translational readthrough is a potential
442 therapeutic strategy for nonsense mutant *TP53*-carrying tumors upon diagnosis, or for
443 prevention of tumors in cancer-prone individuals such as LFS family members carrying
444 an inherited *TP53* nonsense mutation. Given that around 11% of all *TP53* mutations in

445 cancer are nonsense mutations (6), successful clinical implementation of efficient
446 readthrough-inducing therapy would have a significant impact on public health
447 worldwide.
448

449 # Materials and methods

450 **Generation of *Trp53*^{R210X} mutant mice**

451 To generate the *Trp53*^{R210X} mouse model, a chemically modified synthetic single-guide
452 RNA (sgRNA) (5'-gcagacttttCGCcacagcg-3') with an 80-mer SpCas9 scaffold targeting
453 the region encoding the R210 codon in *Trp53* exon 6 was used (CRISPRevolution
454 sgRNA EZ Kit, Synthego, USA). Single strand oligodeoxynucleotides (ssODNs) of 200
455 nucleotides were used as repair template (Ultramer^{TM}, Integrated DNA Technologies,
456 USA; 5'-
457 ctgacttattcttgctcttaggcctggctcctccccagcatcttatccgggtggaaggaaatttgtatcccgagtatctAga
458 agacaggcagacttttTgAcaTagTgtggtggtaccttatgagccacccgaggtctgtaattttgttttggtttgtgcgtct
459 tagagacagttgactccagcctagactgatgttgac-3') for homology-directed repair (HDR). The
460 sequence included silent mutations to exclude recutting of the guide RNA and an XbaI
461 site (tctAga) close to the R210X codon TgA to facilitate genotyping. The CRISPR/Cas9
462 strategy was verified by editing NIH/3T3 mouse fibroblasts (CRL-1658, ATCC, USA),
463 see below for genotyping strategy using the XbaI site. The edited NIH/3T3 cells were
464 plated as single cells and cultured in Dulbecco's Modified Eagle's Medium High
465 Glucose (DMEM) supplemented with 5% FBS.
466

467 The edited mice were produced at the Karolinska Center for Transgene Technologies,
468 Karolinska Institutet. Zygotes harvested from superovulated and mated C57BL/6J
469 female mice (Charles River Laboratories, Germany) were microinjected into the

470 pronuclei with injection buffer [10 mM Tris-HCl (pH 7.5), 0.1 mM EDTA] containing a
471 pre-formed Cas9-sgRNA ribonucleoprotein complex at a concentration of 20 ng/µl
472 eSpCas9 (Sigma-Aldrich/Merck, Germany), 20 ng/µl of the *Trp53* sgRNA (Synthego),
473 and 20 ng/µl of the 200 nucleotide ssODN Ultramer (Integrated DNA Technologies).
474 Microinjected zygotes were implanted into oviducts of pseudopregnant SOPF
475 RjOrl:SWISS (Janvier Labs, France) surrogate female mice via microsurgery. Ear
476 punch biopsies from the F0 offspring were lysed (42) and subjected to PCR with
477 primers encompassing the edited region, giving a 1049 bp amplicon (*Trp53* exon 5-7;
478 Forward primer: 5'-ATCGTTACTCGGCTTGTCCC-3'; Reverse primer: 5'-
479 GGGTAGGAACCAAAGAGCGT-3'). PCR products were purified using the QIAquick
480 PCR Purification Kit (Qiagen, Germany) and digested with restriction enzyme XbaI
481 (New England Biolabs, USA) to reveal recombination of the ssODN template. The PCR
482 amplicons from selected candidate F0 mice were subcloned into pMiniT 2.0 (New
483 England Biolabs) and individual plasmid clones were subjected to Sanger sequencing
484 (KIGene, Karolinska Institutet). All F1 mice identified as heterozygous were further
485 confirmed by Sanger sequencing individual plasmid clones using primers described
486 above for *Trp53* exon 5-7. Sequences were analyzed using the SnapGene (version
487 7.0.1) and Jalview (version 2.11.2.6) softwares.
488
489 **Animal studies**
490 Animal care was in accordance with Swedish regulation and Karolinska Institutet
491 guidelines. Experimental mice were housed in enriched individually ventilated cages
492 in 1 hour dawn/dusk and 10h light/dark cycle, at 22°C ± 2°C and 50% ± 20% air
493 humidity at a pathogen-free animal facility at Karolinska Institutet. Mice were supplied
494 with irradiated CRM(P) mouse pellets (SAFE Diets, France) and drinking water *ad*

495 *libitum*. All animal studies were approved by the Stockholm Regional Animal Ethical
496 Committee, Sweden (Dnr 14188-2019).
497
498 *Trp53*$^{R210X/+}$ mice were maintained on a C57BL/6J background by backcrossing to
499 C57BL/6J mice purchased from Charles River Laboratories. Homozygous mice were
500 generated by intercrossing *Trp53*$^{R210X/+}$ and/or *Trp53*$^{R210X/R210X}$ mice. *Trp53*^{R172H} (9)
501 (C57BL/6J background), a kind gift from Dr. Guillermina Lozano, MD Anderson Cancer
502 Center, Houston, were used as a reference strain. DNA for genotyping was extracted
503 from ear biopsies using the Gentra Puregene Tissue Kit (Qiagen). Genotyping
504 *Trp53*^{R210X} mice was performed by two separate touchdown PCR reactions (10 cycles
505 of touchdown from 65°C to 61°C, followed by 25 cycles at 60°C – total 35 cycles) with
506 specific primers to detect mutant and WT alleles, respectively (*Trp53*-R210X allele,
507 252 bp amplicon, forward primer: 5'-CATCTACAAGAAGTCACAGCAC-3', reverse
508 primer: 5'-GGTACCACCACACTATGTCA-3'; *Trp53*-R210 WT allele, 95 bp amplicon,
509 forward primer: 5'-GCAGACTTTTCGCCACAGC-3', reverse primer: 5'-
510 CTGGAGTCAACTGTCTCTAAGAC-3'). PCR products were analyzed on 2% agarose
511 gels using a Gel Doc EZ Imager system (Bio-Rad Laboratories, USA). Genotyping of
512 *Trp53*^{R172H} mice was performed as described(9). Mice presenting a mutant allele band
513 together with a WT allele band in the genotyping PCR were considered heterozygous,
514 and mice showing only a mutant allele band and no WT band were considered
515 homozygous. Mice from *Trp53*$^{R210X/+}$ intercrosses that were negative for the R210X
516 mutation are referred to as WT mice and were used as controls. *Trp53*^{R210X} mouse
517 bodyweights were recorded weekly from postnatal week 2 and until moribund and
518 euthanized. Homozygous mice were palpated weekly for tumor occurrence starting at

519 10 weeks of age, and heterozygous as well as WT littermate mice were palpated from
520 12 months of age.
521
522 **Tissue collection and processing**
523 Moribund mice were euthanized by cervical dislocation and tissues were directly
524 collected for further analysis. Tissue samples were also collected from mice found
525 dead, unless there was too much autolysis. Tissues for molecular analysis were
526 collected either by immediate snap freezing in liquid nitrogen and stored at -80°C, or
527 in RNAlater™ Stabilizing Solution (Thermo Fisher Scientific, USA). Tissues collected
528 for histological analysis were carefully dissected and fixed in 4% formaldehyde
529 (buffered, pH 6.9, Sigma-Aldrich/Merck) at room temperature on a slow set rocking
530 table for 24-48h, and subsequently transferred to 70% ethanol for storage at 4°C until
531 further use. Skeletal tissues and calcified tumors were decalcified using MolDecal10
532 Ready to use Solution (pH 7.2-7.4, HistoLab Products, Sweden) for 3-4 weeks in 4°C
533 on a slow set rocking table. Decalcification solution was changed every 3-5 days. For
534 establishment of thymic lymphoma cell lines, enlarged thymuses from homozygous
535 mice were fine dissected and collected in ice-cold PBS (see below).
536
537 **Histopathology and immunohistochemistry (IHC)**
538 Formaldehyde-fixed tissues were processed in an automated tissue processing
539 machine (LOGOS, Milestone Medical, Italy) for dehydration, followed by paraffin-
540 embedding and microtome sectioning (4μm). Sections were collected on Superfrost™
541 Plus Adhesion Microscope Slides (Thermo Scientific, USA). For histological analysis,
542 slides were stained with hematoxylin and eosin (HE) using a standard protocol.
543 Verification of tumor cell origin was done by IHC following standard methods. Staining

544 was performed with antibodies against CD3 (1:900, A0452, DAKO/Technologies,
545 USA), desmin (1:2000, ab32362, Abcam, UK), myogenin (1:100, ab124800, Abcam)
546 (all with EDTA pH 8.5 for antigen retrieval), CD68 (1:800, #97778, Cell Signaling
547 Technology, USA), and vimentin (1:1000, ab92547, Abcam) (both with citrate buffer
548 pH 6.0 for antigen retrieval), and incubation at 4°C overnight. Visualization was
549 performed using ImmPress HRP and ImmPACT DAB kits (MP-7401 and SK-4205,
550 Vector Laboratories, USA), followed by counterstaining in Mayer's hematoxylin. HE
551 and IHC slides were examined by light microscopy.
552

553 ***Ex vivo* MRI data acquisition**

554 MRI data were acquired using a 9.4T MRI scanner (Varian, UK) with a horizontal bore.
555 The scanner was controlled with software VnmrJ v4.0 Revision A. A gradient insert
556 with an inner diameter of 12 cm (Varian, UK) and a millipede RF-coil with an inner
557 diameter of 40 mm (Varian) were used. The scan program contained an overview scan,
558 scanner alignment, diffusion weighted, T1-weighted (fat suppressed and Two-point
559 Dixon) and T2-weighted (fat suppressed and FLAIR) scans. Overview and Two-point
560 Dixon sequences were acquired in sagittal plane, the others in dorsal plane. Images
561 were reviewed in collaboration with a European specialist in veterinary diagnostic
562 imaging on a computer workstation using digital imaging and communications in
563 medicine image viewing software (Horos software vers. 3.3.6, Horos project).
564

565 **Assessment of loss of heterozygosity (LOH)**

566 *Trp53*$^{R210X/+}$ tumors collected from euthanized mice were analyzed for LOH by a semi-
567 quantitative method, using the aforementioned genotyping PCR but with only 29 cycles
568 and 100ng DNA per sample. DNA was extracted as described above under Animal

569 studies. For each tumor, tail tissue from the corresponding mouse was used as a
570 control. To quantify the fraction of WT allele left in the tumor, agarose gel band
571 intensities of WT and mutant PCR products were measured for tail and tumor tissue,
572 respectively; analysis was performed using Image Lab Software (Mac Version 6.1, Bio-
573 Rad Laboratories) of gel band signal intensities from gel picture raw data. Tumor
574 intensity ratio was normalized to the respective tail using the following formula:

575 $$\frac{tumorWT/tumorMUT}{tailWT/tailMUT}$$

576 LOH was defined as a value < 0.5, indicating <50% WT allele fraction in tumor
577 compared to tail.

578

579 **Establishment of T-cell lymphoma cell lines**

580 Thymic (T-cell) lymphoma cell lines were established and cultured as described (43).

581

582 **Flow cytometry**

583 T-cell origin of established cell lines was verified by flow cytometry. $5x10^5$ cells were
584 incubated in staining buffer (3% FBS in PBS) containing the following antibodies: Anti-
585 CD3-FITC (1:100, #11-0031-85), Anti-CD4-APC (1:100, #17-0041-83), and Anti-CD8-
586 PE (1:100, #12-0081-85) (all eBioScience, USA). Alive cells were assessed by
587 FxCycle™ Violet Stain DAPI (Thermo Fisher Scientific) diluted 1:500 in staining buffer.
588 Cells were incubated 20 min at 4˚C with 100µl of the antibody/DAPI cocktail, followed
589 by adding 1ml staining buffer and centrifugation at 400g for 5 min. Cells were
590 resuspended in 500µl staining buffer, filtered through a 35µm cell strainer and analyzed
591 using a NovoCyte flow cytometer (ACEA Biosciences, USA).

592

593 Cell death was assessed by Annexin V staining. $5x10^4$ cells/ml were seeded in 6-well-
594 plates using 4ml/well. Cells were treated with G418 (0-200µM) for 72 hours. Treated
595 cells were harvested, washed with DPBS (Sigma-Aldrich/Merck), resuspended in
596 Annexin V binding buffer, counted using Countess 3 Automated Cell Counter (Thermo
597 Fisher Scientific) and diluted to $1x10^6$ cells/ml. 100µl cell dilution was incubated with
598 5µl BD HorizonTM V450 Annexin V antibody (BD Biosciences, USA) for 15 minutes in
599 the dark at room temperature (RT). 400µl Annexin V binding buffer was added and
600 cells were analyzed using a NovoCyte flow cytometer (ACEA Biosciences).
601
602 **Western blotting**
603 T-lymphoma cells were seeded in 6-well-plates at $1\text{-}3x10^5$ cells/ml and treated with
604 G418 (0-200µM) for 72 hours. Western blotting was performed as previously described
605 using 80µg protein (44). Detection of p53 was performed using primary antibody 1C12
606 anti-p53 (1:1000, #2524, Cell Signaling Technology) and an HRP-conjugated Rabbit-
607 anti-Mouse IgG secondary antibody (1:5000, #61-6520, Invitrogen, USA). Following
608 visualization of p53, HRP-conjugated G-9 anti-GAPDH antibody (1:10 000, sc-365062,
609 Santa Cruz Biotechnology, USA) was used as a loading control. Proteins were
610 visualized by SuperSignal™ West Femto Maximum Sensitivity Substrate and iBright
611 FL1000 imaging system (both Thermo Fisher Scientific). All original Western blots are
612 provided in Supplementary Information – Original Western blots.
613
614 **Immunofluorescence staining**
615 $1x10^5$ T-lymphoma cells in 100µl PBS were used for Cytospin (Shandon CYTOSPIN
616 4, Thermo Electron Corporation) at 1500 rpm for 1 min. Cells were fixed in 4%
617 formaldehyde for 10 min at RT, permeabilized using 0.1% Triton in PBS for 5 min at

618 RT, followed by washing in PBS. Primary antibodies rabbit polyclonal p53 N-terminal
619 antibody [N1] (GTX100629, Genetex, USA) and goat polyclonal Anti-TP53 (280aa C-
620 Term) (ASJ-VN4O74-150, Nordic Biosite, Sweden) were diluted together at 1:100 in
621 PBS, incubation 4°C ON. Following PBS wash, secondary antibodies Donkey anti-
622 Rabbit IgG (H+L) Alexa Fluor™ Plus 488 (A32790) and Donkey anti-Goat IgG (H+L)
623 Alexa Fluor™ Plus 555 (A32816) (both Thermo Fisher Scientific) were diluted together
624 at 1:1000 in PBS, incubation 1h in RT. Slides were washed with PBS and mounted
625 with Fluoroshield™ containing DAPI (F6057, Sigma-Aldrich/Merck). An AxioObserver
626 Z1 (Zeiss) microscope was used for imaging.
627
628 **Quantitative real-time PCR (qRT-PCR)**
629 T-lymphoma cells were seeded in 6-well-plates at $5x10^4$ cells/ml and treated with G418
630 (0-150µM) for 72 hours. Cells were harvested and RNA extraction, cDNA synthesis
631 and qRT-PCR were performed as described except that cDNA synthesis was carried
632 out using SuperScript IV (Thermo Fisher Scientific) (27). TaqMan probes used were
633 *p53* (*Trp53*; Mm01731290_g1), *p21* (*Cdkn1a*; Mm00432448_m1), *Bax*
634 (Mm00432051_m1), *Puma* (*Bbc3*; Mm00519268_m1), *Fas* (Mm01204974_m1),
635 *Zmat3* (Mm00494181_m1), and *Gapdh* (Mm99999915_g1).
636
637 **WST-1 assay**
638 T-lymphoma cells were seeded in 6-well-plates at $5x10^4$ cells/ml and treated with G418
639 (0-400µM) for 72 hours. Cells (100µl) were then transferred to a 96-well-plate and 10µl
640 of cell proliferation reagent WST-1 (Roche, Switzerland) were added. Absorbance was
641 determined at 450nm with a Varioskan™ LUX multimode microplate reader (Thermo
642 Scientific) after 30, 45 and 60 minutes incubation in the cell incubator.

643

644 **Statistical analysis**

645 Statistical analysis of numerical data was performed using GraphPad Prism 10
646 (version 10.4.0). Multiple groups were compared using One-way ANOVA, followed by
647 Tukey's multiple comparisons test when all groups were compared to each other, or
648 by Dunnett's multiple comparisons test when all groups were compared to only the
649 control group. Chi-square goodness-of-fit test was used to assess Mendelian
650 inheritance patterns of gender and genotypes. Mouse bodyweight growth curves were
651 analyzed by Mixed-effects analysis with Tukey's multiple comparisons test. Kaplan-
652 Meier mouse survival curves were analyzed by log-rank (Mantel-Cox) test followed by
653 correction for multiple comparisons using the Holm-Šídák method. Categorical data
654 was analyzed using two-sided Fisher's exact test followed by correction for multiple
655 comparisons using the Holm-Šídák method. Group analysis of data from multiple cell
656 lines was performed using repeated measures two-way ANOVA followed by Dunnett's
657 multiple comparisons test, or by two-way Mixed-effects analysis. Statistical
658 significance was defined as $p < 0.05$. Values are presented as mean ± SEM.

659

660 # Acknowledgements

661 We thank Bernhard Schmierer, Karolinska Genome Engineering (KGE) core facility,
662 and Stephan Teglund, Karolinska Center for Transgene Technologies (KCTT), for
663 expert help with generation of the *Trp53*^{R210X} mouse strain; Prof. Guillermina Lozano,
664 MD Anderson Cancer Center, Houston, for kindly sharing the *Trp53*^{R172H} mouse strain
665 used as a reference strain; Anna Malmerfelt at the Histology core facility, Dept. of
666 Oncology-Pathology, Karolinska Institutet, for excellent help with preparation of
667 sections and staining for histopathological analysis; and Alexis Gombert (DVM, IPSAV,

ECVDI Diplomate), at the Diagnostic Imaging Clinic, University Animal Hospital, Swedish University of Agricultural Sciences, Uppsala, for expert help with interpreting and describing the MRI results.

Author contribution

CS, VR, SÖ, AH and KGW designed the experiments. CS, VR, AH, SÖ and ASO performed the experiments. CS created the *Trp53*^{R210X} mouse strain and performed all mouse-related work. VR performed all histopathological assessment and analysis. All authors took part in analysis and interpretation of data. CS, VR, AH and KGW wrote the manuscript. KGW acquired funding for the project.

Ethics

All animal studies were approved by the Stockholm Regional Animal Ethical Committee, Sweden (Dnr 14188-2019).

Funding

This work was supported by grants to KGW from European Research Council (Advanced ERC grant No. 694825-TRANSREAD), the Swedish Research Council (VR 2017-01509; 2021-02064), the Swedish Cancer Fund (Cancerfonden 18 0774; 21 1473 Pj 01 H), the Swedish Childhood Cancer Fund (Barncancerfonden PR2020-0042), and Karolinska Institutet.

Data availability

691 All original data are available upon request. This work does not include any datasets,
692 such as DNA sequences or protein structure data, that have been uploaded in publicly
693 available repositories.
694

695 Additional information

696 Supplementary information is available at Cell Death & Disease's website.
697

698 # References

699 1. Mello SS, Attardi LD. Deciphering p53 signaling in tumor suppression. Curr Opin Cell
700 Biol. 2018;51:65-72.

701 2. Vousden KH, Prives C. Blinded by the Light: The Growing Complexity of p53. Cell.
702 2009;137(3):413-31.

703 3. Andrysik Z, Galbraith MD, Guarnieri AL, Zaccara S, Sullivan KD, Pandey A, et al.
704 Identification of a core TP53 transcriptional program with highly distributed tumor
705 suppressive activity. Genome Res. 2017;27(10):1645-57.

706 4. Kastenhuber ER, Lowe SW. Putting p53 in Context. Cell. 2017;170(6):1062-78.

707 5. Joerger AC, Ang HC, Fersht AR. Structural basis for understanding oncogenic p53
708 mutations and designing rescue drugs. Proceedings of the National Academy of Sciences of
709 the United States of America. 2006;103(41):15056-61.

710 6. Tate JG, Bamford S, Jubb HC, Sondka Z, Beare DM, Bindal N, et al. COSMIC: the
711 Catalogue Of Somatic Mutations In Cancer. Nucleic Acids Res. 2019;47(D1):D941-D7.

712 7. Boettcher S, Miller PG, Sharma R, McConkey M, Leventhal M, Krivtsov AV, et al. A
713 dominant-negative effect drives selection of TP53 missense mutations in myeloid
714 malignancies. Science. 2019;365(6453):599-604.

715 8. Oren M, Rotter V. Mutant p53 gain-of-function in cancer. Cold Spring Harb Perspect
716 Biol. 2010;2(2):a001107.

717 9. Lang GA, Iwakuma T, Suh YA, Liu G, Rao VA, Parant JM, et al. Gain of function of a p53
718 hot spot mutation in a mouse model of Li-Fraumeni syndrome. Cell. 2004;119(6):861-72.

719 10. Muller PA, Caswell PT, Doyle B, Iwanicki MP, Tan EH, Karim S, et al. Mutant p53 drives
720 invasion by promoting integrin recycling. Cell. 2009;139(7):1327-41.

721 11. Lane DP. Mutant p53 Gain-of-Function in the Spotlight: Are We Suffering a GOF
722 Delusion? Cancer Discov. 2024;14(2):211-3.

723 12. Wang Z, Burigotto M, Ghetti S, Vaillant F, Tan T, Capaldo BD, et al. Loss-of-Function but
724 Not Gain-of-Function Properties of Mutant TP53 Are Critical for the Proliferation, Survival, and
725 Metastasis of a Broad Range of Cancer Cells. Cancer Discov. 2024;14(2):362-79.

726 13. Funk JS, Klimovich M, Drangenstein D, Pielhoop O, Hunold P, Borowek A, et al. Deep
727 CRISPR mutagenesis characterizes the functional diversity of TP53 mutations. Nature genetics.
728 2025;57(1):140-53.

729 14. Shirole NH, Pal D, Kastenhuber ER, Senturk S, Boroda J, Pisterzi P, et al. TP53 exon-6
730 truncating mutations produce separation of function isoforms with pro-tumorigenic
731 functions. Elife. 2016;5.

732 15. Donehower LA, Harvey M, Slagle BL, McArthur MJ, Montgomery CA, Jr., Butel JS, et al.
733 Mice deficient for p53 are developmentally normal but susceptible to spontaneous tumours.
734 Nature. 1992;356(6366):215-21.

735 16. Jacks T, Remington L, Williams BO, Schmitt EM, Halachmi S, Bronson RT, et al. Tumor
736 spectrum analysis in p53-mutant mice. Curr Biol. 1994;4(1):1-7.

737 17. Olive KP, Tuveson DA, Ruhe ZC, Yin B, Willis NA, Bronson RT, et al. Mutant p53 gain of
738 function in two mouse models of Li-Fraumeni syndrome. Cell. 2004;119(6):847-60.

739 18. Lee MK, Teoh WW, Phang BH, Tong WM, Wang ZQ, Sabapathy K. Cell-type, dose, and
740 mutation-type specificity dictate mutant p53 functions in vivo. Cancer Cell. 2012;22(6):751-
741 64.

742 19. Gencel-Augusto J, Su X, Qi Y, Whitley EM, Pant V, Xiong S, et al. Dimeric p53 Mutant
743 Elicits Unique Tumor-Suppressive Activities through an Altered Metabolic Program. Cancer
744 Discov. 2023;13(5):1230-49.

745 20. Xiong S, Chachad D, Zhang Y, Gencel-Augusto J, Sirito M, Pant V, et al. Differential Gain-
746 of-Function Activity of Three p53 Hotspot Mutants In Vivo. Cancer Res. 2022;82(10):1926-36.

747 21. Tang J, Feng Y, Kuick R, Green M, Green M, Sakamoto N, et al. Trp53 null and R270H
748 mutant alleles have comparable effects in regulating invasion, metastasis, and gene
749 expression in mouse colon tumorigenesis. Lab Invest. 2019;99(10):1454-69.

750 22. Floquet C, Deforges J, Rousset JP, Bidou L. Rescue of non-sense mutated p53 tumor
751 suppressor gene by aminoglycosides. Nucleic Acids Res. 2011;39(8):3350-62.

752 23. Friesen WJ, Trotta CR, Tomizawa Y, Zhuo J, Johnson B, Sierra J, et al. The nucleoside
753 analog clitocine is a potent and efficacious readthrough agent. RNA. 2017;23(4):567-77.

754 24. Crawford DK, Alroy I, Sharpe N, Goddeeris MM, Williams G. ELX-02 Generates Protein
755 via Premature Stop Codon Read-Through without Inducing Native Stop Codon Read-Through
756 Proteins. J Pharmacol Exp Ther. 2020;374(2):264-72.

757 25. Trzaska C, Amand S, Bailly C, Leroy C, Marchand V, Duvernois-Berthet E, et al. 2,6-
758 Diaminopurine as a highly potent corrector of UGA nonsense mutations. Nat Commun.
759 2020;11(1):1509.

760 26. Baradaran-Heravi A, Balgi AD, Hosseini-Farahabadi S, Choi K, Has C, Roberge M. Effect
761 of small molecule eRF3 degraders on premature termination codon readthrough. Nucleic
762 Acids Res. 2021;49(7):3692-708.

763 27. Palomar-Siles M, Heldin A, Zhang M, Strandgren C, Yurevych V, van Dinter JT, et al.
764 Translational readthrough of nonsense mutant TP53 by mRNA incorporation of 5-
765 Fluorouridine. Cell Death Dis. 2022;13(11):997.

766 28. Kan Y, Ruis B, Takasugi T, Hendrickson EA. Mechanisms of precise genome editing using
767 oligonucleotide donors. Genome Res. 2017;27(7):1099-111.

768 29. Pettan-Brewer C, Treuting PM. Practical pathology of aging mice. Pathobiol Aging Age
769 Relat Dis. 2011;1.

770 30. Zhang M, Heldin A, Palomar-Siles M, Ohlin S, Bykov VJN, Wiman KG. Synergistic Rescue
771 of Nonsense Mutant Tumor Suppressor p53 by Combination Treatment with Aminoglycosides
772 and Mdm2 Inhibitors. Front Oncol. 2018;7:323.

773 31. Hu W, Feng Z, Teresky AK, Levine AJ. p53 regulates maternal reproduction through LIF.
774 Nature. 2007;450(7170):721-4.

775 32. Sah VP, Attardi LD, Mulligan GJ, Williams BO, Bronson RT, Jacks T. A subset of p53-
776 deficient embryos exhibit exencephaly. Nature genetics. 1995;10(2):175-80.

777 33. Armstrong JF, Kaufman MH, Harrison DJ, Clarke AR. High-frequency developmental
778 abnormalities in p53-deficient mice. Curr Biol. 1995;5(8):931-6.

779 34. Kim U, Kim CY, Oh H, Lee JM, Chang SN, Ryu B, et al. Phenotyping analysis of p53
780 knockout mice produced by gene editing and comparison with conventional p53 knockout
781 mice. Genes Genomics. 2019;41(6):701-12.

782 35. Tateossian H, Morse S, Simon MM, Dean CH, Brown SD. Interactions between the otitis
783 media gene, Fbxo11, and p53 in the mouse embryonic lung. Dis Model Mech.
784 2015;8(12):1531-42.

785 36. Elies L, Guillaume E, Gorieu M, Neves P, Schorsch F. Historical Control Data of
786 Spontaneous Pathological Findings in C57BL/6J Mice Used in 18-Month Dietary
787 Carcinogenicity Assays. Toxicol Pathol. 2024;52(2-3):99-113.

788 37. Janke LJ, Rehg JE. The many faces of mouse histiocytic sarcoma in C57BL/6J mice. Vet
789 Pathol. 2023;60(4):443-60.

790 38. Willard-Mack CL, Elmore SA, Hall WC, Harleman J, Kuper CF, Losco P, et al.
791 Nonproliferative and Proliferative Lesions of the Rat and Mouse Hematolymphoid System.
792 Toxicol Pathol. 2019;47(6):665-783.

793 39. Venkatachalam S, Shi YP, Jones SN, Vogel H, Bradley A, Pinkel D, et al. Retention of
794 wild-type p53 in tumors from p53 heterozygous mice: reduction of p53 dosage can promote
795 cancer formation. EMBO J. 1998;17(16):4657-67.

796 40. Cooper TK, Meyerholz DK, Beck AP, Delaney MA, Piersigilli A, Southard TL, et al.
797 Research-Relevant Conditions and Pathology of Laboratory Mice, Rats, Gerbils, Guinea Pigs,
798 Hamsters, Naked Mole Rats, and Rabbits. ILAR J. 2021;62(1-2):77-132.

799 41. de Andrade KC, Lee EE, Tookmanian EM, Kesserwan CA, Manfredi JJ, Hatton JN, et al.
800 The TP53 Database: transition from the International Agency for Research on Cancer to the
801 US National Cancer Institute. Cell Death Differ. 2022;29(5):1071-3.

802 42. Truett GE, Heeger P, Mynatt RL, Truett AA, Walker JA, Warman ML. Preparation of
803 PCR-quality mouse genomic DNA with hot sodium hydroxide and tris (HotSHOT).
804 Biotechniques. 2000;29(1):52, 4.

805 43. Jinadasa R, Balmus G, Gerwitz L, Roden J, Weiss R, Duhamel G. Derivation of thymic
806 lymphoma T-cell lines from Atm(-/-) and p53(-/-) mice. J Vis Exp. 2011(50).

807 44. Heldin A, Cancer M, Palomar-Siles M, Ohlin S, Zhang M, Sun-Zhang A, et al. Novel
808 compounds that synergize with aminoglycoside G418 or eRF3 degraders for translational
809 readthrough of nonsense mutant TP53 and PTEN. RNA Biol. 2023;20(1):368-83.

810

811

812 # Figure legends

813 **Figure 1. Generation of the *Trp53*^{R210X} knock-in mouse strain. (A)** Schematic
814 representation of the CRISPR/Cas9 strategy for generation of *Trp53*^{R210X} mutant mice.
815 A single-guide RNA (sgRNA) was designed to target the region encoding the R210
816 codon in *Trp53* exon 6. The expected cleavage site is 3 nucleotides upstream of the
817 Protospacer Adjacent Motif (PAM) sequence. The donor single-stranded

818 oligodeoxynucleotide (ssODN) template was designed to introduce nucleotide
819 replacements resulting in an Arg (CGC) to STOP (TGA) substitution (indicated in red)
820 at codon 210 (R210X), and an XbaI cut site to facilitate genotyping by restriction
821 enzyme digestion (introduced nucleotide shown in green). Silent mutations introduced
822 to prevent recutting of the sgRNA are shown in orange. The figure is not to scale. **(B)**
823 Representative results from sequence analysis of plasmid clones from edited NIH/3T3
824 cell clones, showing a correct R210X sequence but inconsistent introduction of the
825 XbaI site. **(C)** Genotyping strategy using wildtype (WT) and mutation specific primers
826 for PCR amplification. PCR products were run on a 2% agarose gel. WT allele is
827 identified by a 95 bp PCR fragment (top panel), and mutant allele by a 252 bp PCR
828 fragment (bottom panel). **(D)** Representative chromatograms showing clean WT
829 (upper panel) and mutated (lower panel) *Trp53* sequences from heterozygous F1 mice,
830 indicating successful knock-in of desired mutations and germline transmission of the
831 R210X allele. Altered nucleotides producing the STOP codon (TGA) at amino acid
832 position 210 are shown in red, silent mutations are shown in orange.
833
834 **Figure 2. Female *Trp53*$^{R210X/R210X}$ mice are significantly lighter and *Trp53*^{R210X}**
835 **mice have a reduced lifespan.** Bodyweight development of female **(A)** and male **(B)**
836 *Trp53*$^{R210X/+}$ and *Trp53*$^{R210X/R210X}$ mice as compared to wildtype (WT) littermates. **(A)**
837 Female *Trp53*$^{R210X/R210X}$ mice were significantly lighter during their whole lifespan as
838 compared to *Trp53*$^{R210X/+}$ and WT littermates (****$p < 0.0001$). **(B)** Male mice of the
839 different genotypes showed no bodyweight differences until 34 weeks of age. From
840 this point, at the end of their maximum lifespan, male *Trp53*$^{R210X/R210X}$ mice were
841 significantly lighter than *Trp53*$^{R210X/+}$ and WT littermates (****$p < 0.0001$). Indicated *n*-
842 values are the total number of mice monitored from 2 weeks of age. Only weights from

843 mice scored as healthy according to general health assessment are shown in **A-B**, as
844 a mouse with tumor burden tends to either dramatically lose weight or gain weight. **(C-**
845 **E)** Kaplan-Meier curves illustrating the effects of the *Trp53*^{R210X} mutation on survival.
846 WT littermates and *Trp53*^{R172H} missense mutant knock-in mice are shown for
847 comparison. All inter-strain comparisons between different genotypes of both
848 *Trp53*^{R210X} and *Trp53*^{R172H} strains were highly significant (adj. P-values: p = 0.0008)
849 (WT vs. heterozygous; WT vs. homozygous; heterozygous vs. homozygous); only P-
850 values for comparison of *Trp53*$^{R210X/+}$ and *Trp53*$^{R172H/+}$ mice are indicated in the figure.
851 **(C)** Male *Trp53*$^{R210X/+}$ mice showed significantly longer survival compared to
852 *Trp53*$^{R172H/+}$ mice (adj. P-value: p = 0.013), but the difference between the female
853 heterozygous mice of the two strains was not statistically significant **(D)**. **(E)** When
854 male and female mouse survival data were combined, *Trp53*$^{R210X/+}$ mice lived
855 significantly longer than *Trp53*$^{R172H/+}$ mice (adj. P-value: p = 0.01). There was no
856 difference in the survival between *Trp53*$^{R210X/R210X}$ and *Trp53*$^{R172H/R172H}$ mice of either
857 sex, or when data for male and female mice were combined. **(F-G)** Comparison of
858 male and female survival of the different genotypes showed significant differences for
859 *Trp53*$^{R210X/+}$ mice (p = 0.003) and WT mice (p = 0.043). Black ticks in panels **C-G**
860 indicate mice that have been censored (i.e. euthanized due to non-cancer related
861 reasons such as wounds from scratching/over-grooming or malocclusion). Bodyweight
862 growth curves in **A** and **B** were analyzed by Mixed-effects analysis with Tukey's
863 multiple comparisons test. Values represent the mean ± SEM. Survival curves in **C-G**
864 were analyzed by log-rank (Mantel-Cox) test followed by correction for multiple
865 comparisons using the Holm-Šídák method when applicable (**C-E**). P-values: *p <
866 0.05, **p < 0.01, ***p < 0.001, ****p < 0.0001.
867

868 **Figure 3. *Trp53*$^{R210X/R210X}$ mice develop multicentric lymphomas and sarcomas.**
869 Examples of tumors observed at necropsy and their histopathological diagnosis. All
870 necropsy photographs are oriented with the head at the top. All histomicrographs are
871 stained with hematoxylin-eosin (HE) or immunohistochemistry (IHC) as indicated.
872 Scale bars = 20μm. Red stars = mitotic figures; red arrows = single-cell death; black
873 arrows = tingible body macrophage; purple arrows = cytoplasmic staining; black stars
874 = nuclear staining. **(A1)** A male *Trp53*$^{R210X/R210X}$ mouse with a severely enlarged
875 thymus (T). **(A2)** Histomicrograph of the thymus neoplasia in A1. The normal thymus
876 architecture is completely effaced by mats of neoplastic round cells with dispersed
877 tingible body macrophages phagocytosing dead neoplastic cells (arrows). **(A3)** CD3
878 IHC confirming that the neoplastic lymphocytes are T-cells. **(A4)** Histomicrograph of
879 lung shown in A1 with perivascular neoplastic lymphocyte infiltrates, L indicates
880 unaffected lung tissue. **(B1)** A male *Trp53*$^{R210X/R210X}$ mouse with a severely enlarged
881 spleen (S) and liver (Li). **(B2)** Histomicrograph of spleen shown in B1. The normal
882 splenic architecture is completely effaced by mats of neoplastic round cells. **(B3)** CD3
883 IHC confirming that the neoplastic lymphocytes are T-cells. **(B4)** Histomicrograph of
884 liver shown in B1, with severe perivascular and intrasinusoidal neoplastic lymphocyte
885 infiltrates, H indicates hepatocytes. **(C1)** A male *Trp53*$^{R210X/R210X}$ mouse with a
886 subcutaneous tumor on the left side of thorax and abdomen. **(C2)** Histomicrograph of
887 the subcutaneous tumor in C1, with a dense proliferation of pleomorphic neoplastic
888 mesenchymal cells forming streams and bundles. Black arrowhead indicates a giant
889 cell with a bizarre, giant nucleus. **(C3 and C4)** Desmin and myogenin IHC confirming
890 that the neoplastic cells originate from skeletal muscle. **(D)** Distribution of tumors and
891 multicentric or metastasizing tumors in *Trp53*$^{R210X/R210X}$ mice. The total number of mice
892 includes all mice with at least one tumor. To increase clarity, pleomorphic lymphoma

893 and histiocytic sarcoma were only included when they were the only diagnosed
894 tumor(s), not when they occurred concurrently with other tumor types. Therefore, the
895 number of multicentric tumors are lower than in Supplementary Table S3. The full data
896 is presented in Supplementary Tables S4A and S4D. HS = histiocytic sarcoma;
897 Leiomyo = leiomyosarcoma; Lymph = lymphoma; mc = multicentric; met = metastatic;
898 Pleo lymph = pleomorphic lymphoma; Rhabdo = rhabdomyosarcoma; Sarc = sarcoma.
899
900 **Figure 4. *Trp53*$^{R210X/+}$ mice develop a wide spectrum of tumors with frequent LOH**
901 **and high rate of multicentric and metastatic tumors.** Examples of tumors observed
902 at necropsy and their histopathological diagnosis. All necropsy photographs are
903 oriented with the head at the top. All histomicrographs are stained with hematoxylin-
904 eosin (HE). Scale bars = 20μm. Red stars = mitotic figures, red arrowheads =
905 neoplastic osteoid; green arrows = multinucleate neoplastic cells; purple arrows =
906 cytoplasmic staining; black stars = nuclear staining. **(A1)** A female *Trp53*$^{R210X/+}$ mouse
907 with a hard tumor (O = osteosarcoma) on the thorax wall, involving several ribs. **(A2)**
908 Histomicrograph of the hard tumor in A1, with dense proliferation of very pleomorphic,
909 neoplastic round to spindle-shaped mesenchymal cells that produce variable amounts
910 of neoplastic osteoid, confirming osteosarcoma diagnosis. **(A3)** Histomicrograph of
911 lung from the animal shown in A1, with a large intravascular osteosarcoma metastasis
912 (IvO) adhering to the vessel wall (L = lung parenchyma, Alv = alveolus). **(B1)** A male
913 *Trp53*$^{R210X/+}$ mouse with a hindleg muscle tumor (indicated by the white line). **(B2)**
914 Histomicrograph of the tumor from the animal shown in B1. Short streams and bundles
915 of highly pleomorphic, spindle-shaped to polygonal neoplastic mesenchymal cells in a
916 minimal stroma, with numerous multinucleate cells. **(B3 and B4)** Positive cytoplasmic
917 desmin and nuclear myogenin immunohistochemistry confirming that the neoplastic

918 cells originate from skeletal muscle. **(C1)** A male *Trp53*$^{R210X/+}$ mouse with numerous
919 severely enlarged peripheral lymph nodes (Submand L = submandibular lymph nodes;
920 Ax L = axillar lymph nodes; Ing L = inguinal lymph nodes). Inset shows lungs *in situ.*
921 **(C2 and C3)** Histomicrographs of a lymph node and the spleen from the animal shown
922 in C1, with dense proliferation of neoplastic round cells variably effacing the normal
923 tissue architecture i.e. lymphoma. **(C4-C6)** Histomicrographs of lung, liver and kidney
924 from the animal shown in C1, with perivascular and interstitial neoplastic infiltrates, i.e.
925 metastatic lymphoma (**C4**: Alv = alveolus, V = blood vessel lumen, L = lung
926 parenchyma; **C5**: Li = liver parenchyma; **C6**: Ki = kidney parenchyma). **(D)** Distribution
927 and combinations of tumors and multicentric or metastasizing tumors found in
928 *Trp53*$^{R210X/+}$ mice. The total number of mice includes all mice with at least one tumor.
929 To increase clarity, pleomorphic lymphoma and histiocytic sarcoma were only included
930 when they were the only diagnosed tumor(s), not when they occurred concurrently with
931 other tumor types. Therefore, the number of multicentric tumors are lower than in
932 Supplementary Table S3. The full data is presented in Supplementary Tables S4B and
933 S4D. Ad = adenoma; Ca = carcinoma; Hemangio = hemangiosarcoma; HS = histiocytic
934 sarcoma; Leiomyo = leiomyosarcoma; Lymph = lymphoma; mc = multicentric;
935 Mesothel = mesothelioma; met = metastatic; Osteo = osteosarcoma; Pleo lymph =
936 pleomorphic lymphoma; Rhabdo = rhabdomyosarcoma; Sarc = sarcoma. **(E)**
937 Representative agarose gel for evaluation of LOH in tumors collected from four
938 different euthanized mice. Each animal's tail was used as a control tissue. WT (upper
939 panel) and R210X (lower panel) gel band intensities were measured to quantify the
940 percentage of WT allele retained in each tumor compared to the tail; percentage of
941 retained WT allele in each sample is indicated at the bottom of the panel. LOH was
942 defined as <50% WT allele retained. N = no LOH; Y = LOH.

943

944 **Figure 5. Comparison of tumor spectra of *Trp53*$^{R210X/R210X}$, *Trp53*$^{R210X/+}$ and WT**
945 **mice. (A)** Most frequently found tumor types of hematopoietic, mesenchymal,
946 epithelial and sex cord origin in the three genotypes. *Trp53*$^{R210X/R210X}$ mice showed a
947 high rate of T-cell lymphoma whereas *Trp53*$^{R210X/+}$ was the only genotype that
948 developed osteosarcomas and malignant sex cord tumors. Only *Trp53*$^{R210X/R210X}$ and
949 *Trp53*$^{R210X/-}$ developed soft-tissue sarcomas. Tumor type in bold = found in C57BL/6J
950 WT (i.e.: pleomorphic lymphoma; lymphoma, NOS; histiocytic sarcoma; sarcoma,
951 NOS; other mesenchymal tumors; other carcinomas; benign epithelial tumors) (36);
952 tumor type in italics = several tumor types grouped together; full tumor spectrum is
953 shown in Supplementary Fig. S5A. **(B)** Predominant lymphoma subtypes in
954 *Trp53*$^{R210X/R210X}$, *Trp53*$^{R210X/+}$ and WT mice. TCL = T-cell lymphoma; mc = multicentric;
955 NOS = not otherwise specified; Pleo lymph = pleomorphic lymphoma. *Trp53*$^{R210X/R210X}$
956 had frequent solitary and multicentric thymic T-cell lymphoma while *Trp53*$^{R210X/+}$ and
957 WT mice mainly developed solitary and multicentric pleomorphic lymphomas. **(C)**
958 Distribution of the tumor types unique to the *Trp53*^{R210X} mice, i.e. never found in the
959 WT mice, and never or rarely reported as spontaneous tumors in C57BL6/J mice (36).
960 T-cell lymphoma was more frequent in *Trp53*$^{R210X/R210X}$ than in *Trp53*$^{R210X/+}$ mice, and
961 osteosarcoma was more frequent in *Trp53*$^{R210X/+}$ mice. In both genotypes, the most
962 common myosarcoma was leiomyosarcoma. In *Trp53*$^{R210X/+}$ mice, leiomyosarcomas
963 were as common as osteosarcomas, and both these tumors were more common than
964 all other unique tumors. **(D)** Comparison of tumor spectra in female and male
965 *Trp53*$^{R210X/+}$ mice. Female *Trp53*$^{R210X/+}$ had more frequent osteosarcomas than males.
966 Comparisons of tumor spectra in female and male *Trp53*$^{R210X/R210X}$ and WT mice are
967 shown in Supplementary Fig. S5B-C. **(E-G)** A male *Trp53*$^{R210X/R210X}$ mouse was

968 sacrificed at 234 days of age due to weight loss, strained breath and a neoplasia on
969 the throat, and subjected to an *ex vivo* MRI analysis without prior necropsy. **(E and F)**
970 The throat neoplasia was part of a large neoplastic thymus (outlined by yellow arrows,
971 size approx. 2.7x1.3x0.9 cm) that intrathoracally extended caudally to the diaphragm
972 (indicated by a white arrow in **E**), cranially through the thoracic inlet along the ventral
973 neck to the level of the ramus mandibularis, and extending into the right-side
974 musculature medial to the shoulder, probably involving the prescapular lymph node. In
975 the right cranial mediastinum there was a neoplastically transformed cranial
976 mediastinal lymph node, about 0.8 cm long and 0.4 cm in diameter. The submandibular
977 lymph nodes were not identifiable and appeared to be continuous with the thymus
978 tumor. The lungs had a clear appearance with no signs of neoplastic proliferations or
979 infiltrates. **(G)** In the dorsal abdomen there were multiple enlarged lymph nodes, up to
980 3 mm in diameter, elongated and convoluted (outlined by white arrows). The spleen
981 was mildly enlarged and rounded (not visible in the figure), and in the normal-sized
982 liver there were two nodules with an appearance best consistent with areas of vacuolar
983 degeneration and extramedullary hyperplasia. Statistical analysis in **A-D** was
984 performed by two-sided Fisher's exact test, followed by correction for multiple
985 comparisons using the Holm-Šídák method. In **A**, comparisons were made between
986 genotypes within each tumor type. In **B-C**, comparisons were made between all tumor
987 types within one genotype, and between the different genotypes for each individual
988 tumor type. In **D**, comparisons were made between female and male for each tumor
989 type (i.e. female osteosarcoma vs. male osteosarcoma), and between all tumor types
990 within one sex (i.e. all tumor types found in females). Adjusted P-values: *$p < 0.05$, **p
991 < 0.01; ***$p < 0.001$.
992

993 **Figure 6. Impact of multicentricity, metastasis and thymus size on overall**
994 **survival of *Trp53*$^{R210X/R210X}$ and *Trp53*$^{R210X/+}$ mice. (A)** Kaplan-Meier curves showing
995 that *Trp53*$^{R210X/+}$ mice with multicentric or metastatic disease had significantly better
996 survival compared to mice with solitary tumors (**p* = 0.0167), whereas *Trp53*$^{R210X/R210X}$
997 mice did not (*p* = 0.0595). **(B)** *Trp53*$^{R210X/R210X}$ and *Trp53*$^{R210X/+}$ mice with the indicated
998 malignant solitary tumors (most common solitary tumor types for respective strain) did
999 not show any differences in survival compared to mice of the same genotype with other
1000 solitary tumors. Note that two *Trp53*$^{R210X/R210X}$ mice that were euthanized due to solitary
1001 leiomyosarcoma also had solitary thymic T-cell lymphoma and were included as
1002 solitary thymic T-cell lymphoma in Fig. 5B. Here, however, they are included as "other
1003 solitary malignant tumors" since that was the cause for euthanasia. **(C)**.
1004 *Trp53*$^{R210X/R210X}$ mice with solitary T-cell lymphomas showed significantly shorter
1005 survival than *Trp53*$^{R210X/R210X}$ mice with multicentric or metastatic disease (*p* = 0.0424)
1006 but not compared to mice with sarcomas. Note that two *Trp53*$^{R210X/R210X}$ mice that were
1007 euthanised due to solitary leiomyosarcoma also had solitary thymic T-cell lymphoma
1008 and were included as solitary thymic T-cell lymphoma in Fig. 5B. Here, however, they
1009 are included as "myosarcoma or sarcoma NOS" since that was the cause for
1010 euthanasia. **(D)** *Trp53*$^{R210X/R210X}$ mice with thymic T-cell lymphoma had a shorter
1011 overall survival compared to *Trp53*$^{R210X/R210X}$ mice with T-cell lymphoma in both thymus
1012 and spleen (adj. P-value: *p* = 0.038). **(E)** The thymi of *Trp53*$^{R210X/R210X}$ mice with solitary
1013 thymic T-cell lymphoma were in general larger than the thymi from *Trp53*$^{R210X/R210X}$
1014 mice with T-cell lymphoma in the spleen or in both thymus and spleen. Mean ± SEM
1015 are indicated. Survival curves in **A-D** were analyzed by log-rank (Mantel-Cox) test
1016 followed by correction for multiple comparisons using the Holm-Šídák method when
1017 applicable. In **D,** comparisons were made to the group with solitary thymic lymphoma.

1018 In **E**, statistical analysis was performed using One-way ANOVA followed by Tukey's
1019 multiple comparisons tests. P-values: *$p < 0.05$, **$p < 0.01$; ***$p < 0.001$.
1020
1021 **Figure 7. G418 induces translational readthrough and full-length functional p53**
1022 **in *Trp53*$^{R210X/R210X}$ T-lymphoma cells. (A)** Representative histomicrographs of the
1023 thymus from the *Trp53*$^{R210X/R210X}$ mouse X405 stained with HE (left) and CD3 antibody
1024 (IHC, right). Mats of CD3-positive, i.e. T-cell origin, pleomorphic neoplastic
1025 lymphocytes with numerous mitoses (asterisks), and dispersed, moderate numbers of
1026 tingible body macrophages (arrows) efface the normal thymic architecture. Scale bars
1027 = 50µm. **(B)** Flow cytometry to verify T-cell origin of X405 cells derived from a
1028 *Trp53*$^{R210X/R210X}$ thymic lymphoma by staining with antibodies for CD3 (left panel), and
1029 CD4 and CD8 (right panel). **(C)** Immunofluorescence staining of X405 T-lymphoma
1030 cells, either untreated (0µM G418, left panels) or treated with 100µM G418 (right
1031 panels) for 72 hours. p53 was detected using N1 (N-terminal epitope) and 280aa C-
1032 term (C-terminal epitope) antibodies. Bottom panels show merged DAPI and 280aa C-
1033 term p53 staining, highlighting translational readthrough of the *Trp53*-R210X nonsense
1034 mutation and production of full-length p53 protein upon treatment with G418. Scale
1035 bars = 100µm. **(D)** Western blot analysis showing dose-dependent induction of full-
1036 length p53 in X405 T-lymphoma cells following 72h treatment with G418 at indicated
1037 concentrations. p53 was visualized using the anti-p53 antibody 1C12 that recognizes
1038 an N-terminal epitope and therefore detects both full-length and C-terminally truncated
1039 p53. Gapdh was used as a loading control. **(E)** qRT-PCR analysis showing dose-
1040 dependent induction of *p53* mRNA and p53 target gene mRNA levels in the three
1041 *Trp53*$^{R210X/R210X}$ T-lymphoma cell lines X405, X491 and X547 after 72h treatment with
1042 G418 (upper panel). Two independently established *Trp53*$^{R172H/R172H}$ T-lymphoma cell

1043 lines were used as negative control (lower panel). Gene expression values were
1044 normalized to *Gapdh* expression and compared to the untreated (0μM G418) negative
1045 control for each gene. Each dot represents the mean from three independent
1046 experiments per cell line. **(F)** WST-1 assay to determine proliferation of T-lymphoma
1047 cells from *Trp53*$^{R210X/R210X}$ (n = 3 cell lines) and *Trp53*$^{R172H/R172H}$ (n = 2 cell lines) mice
1048 upon 72h treatment with indicated concentrations of G418. Each dot represents the
1049 mean from eight independent experiments per cell line. **(G)** Flow cytometry of Annexin
1050 V staining to assess apoptotic cell death in *Trp53*$^{R210X/R210X}$ (n = 3 cell lines) and
1051 *Trp53*$^{R172H/R172H}$ (n = 2 cell lines) T-lymphoma cells following 72h treatment with G418.
1052 All quantifications from three independent experiments per cell line are shown.
1053 Statistical analysis was performed by repeated measures two-way ANOVA followed
1054 by Dunnett's multiple comparisons test **(E)**, and by two-way Mixed-effects analysis **(F-**
1055 **G)**, respectively. All individual cell line values from all experiments were used for
1056 statistical analysis but mean ± SEM are indicated in figures **E** and **F**. Adjusted P-values:
1057 *$p < 0.05$, **$p < 0.01$, ***$p < 0.001$, ****$p < 0.0001$.

Figure 1

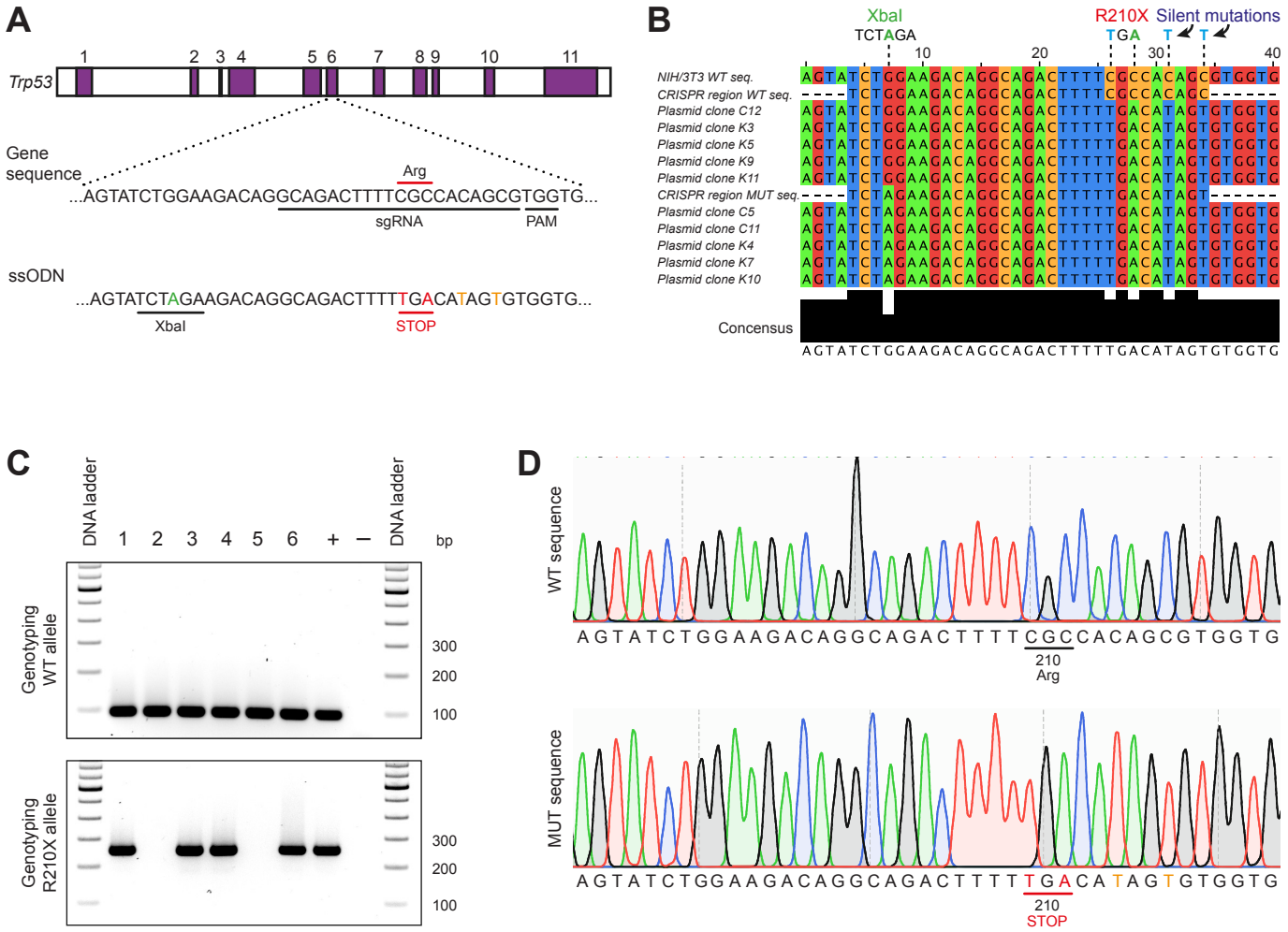
A
Trp53
1 2 3 4 5 6 7 8 9 10 11
Gene sequence
Arg
...AGTATCTGGAAGACAGGCAGACTTTTCGCCACAGCGTGGTG...
sgRNA
PAM
ssODN
...AGTATCTAGAAGACAGGCAGACTTTTTGACATAGTGTGGTG...
XbaI
STOP
B
XbaI
TCTAGA
R210X
Silent mutations
TGA
T
T
10
20
30
40
NIH/3T3 WT seq.
CRISPR region WT seq.
Plasmid clone C12
Plasmid clone K3
Plasmid clone K5
Plasmid clone K9
Plasmid clone K11
CRISPR region MUT seq.
Plasmid clone C5
Plasmid clone C11
Plasmid clone K4
Plasmid clone K7
Plasmid clone K10
Concensus
AGTATCTGGAAGACAGGCAGACTTTTTGACATAGTGTGGTG
C
DNA ladder
1 2 3 4 5 6 + −
DNA ladder
bp
Genotyping WT allele
300
200
100
Genotyping R210X allele
300
200
100
D
WT sequence
AGTATCTGGAAGACAGGCAGACTTTTCGCCACAGCGTGGTG
210
Arg
MUT sequence
AGTATCTGGAAGACAGGCAGACTTTTTGACATAGTGTGGTG
210
STOP

Figure 2

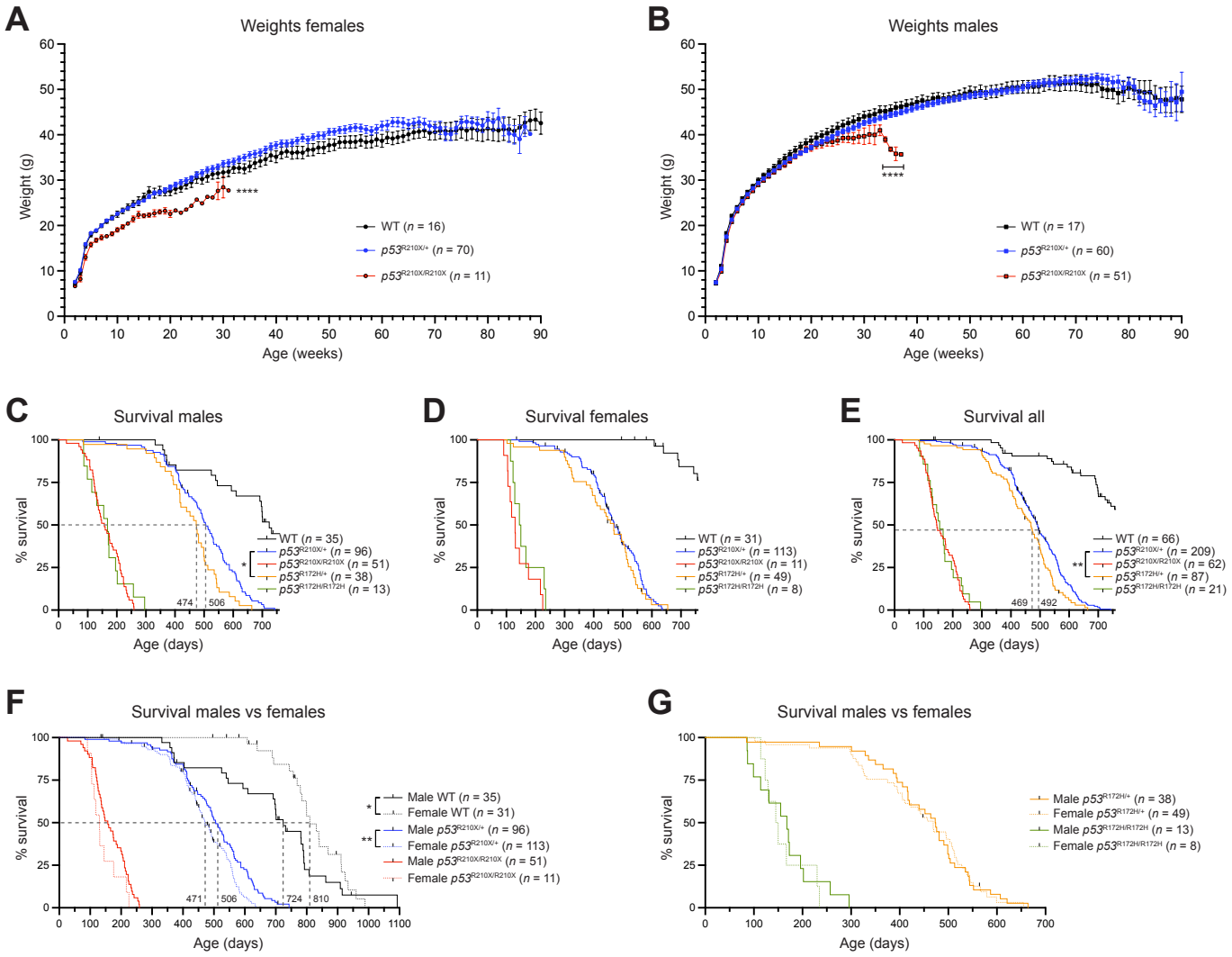
A
Weights females
Weight (g)
Age (weeks)
****
WT (n = 16)
p53R210X/+ (n = 70)
p53R210X/R210X (n = 11)
B
Weights males
Weight (g)
Age (weeks)
****
WT (n = 17)
p53R210X/+ (n = 60)
p53R210X/R210X (n = 51)
C
Survival males
% survival
Age (days)
474
506
*
WT (n = 35)
p53R210X/+ (n = 96)
p53R210X/R210X (n = 51)
p53R172H/+ (n = 38)
p53R172H/R172H (n = 13)
D
Survival females
% survival
Age (days)
WT (n = 31)
p53R210X/+ (n = 113)
p53R210X/R210X (n = 11)
p53R172H/+ (n = 49)
p53R172H/R172H (n = 8)
E
Survival all
% survival
Age (days)
469
492
**
WT (n = 66)
p53R210X/+ (n = 209)
p53R210X/R210X (n = 62)
p53R172H/+ (n = 87)
p53R172H/R172H (n = 21)
F
Survival males vs females
% survival
Age (days)
471
506
724
810
*
**
Male WT (n = 35)
Female WT (n = 31)
Male p53R210X/+ (n = 96)
Female p53R210X/+ (n = 113)
Male p53R210X/R210X (n = 51)
Female p53R210X/R210X (n = 11)
G
Survival males vs females
% survival
Age (days)
Male p53R172H/+ (n = 38)
Female p53R172H/+ (n = 49)
Male p53R172H/R172H (n = 13)
Female p53R172H/R172H (n = 8)

Figure 3

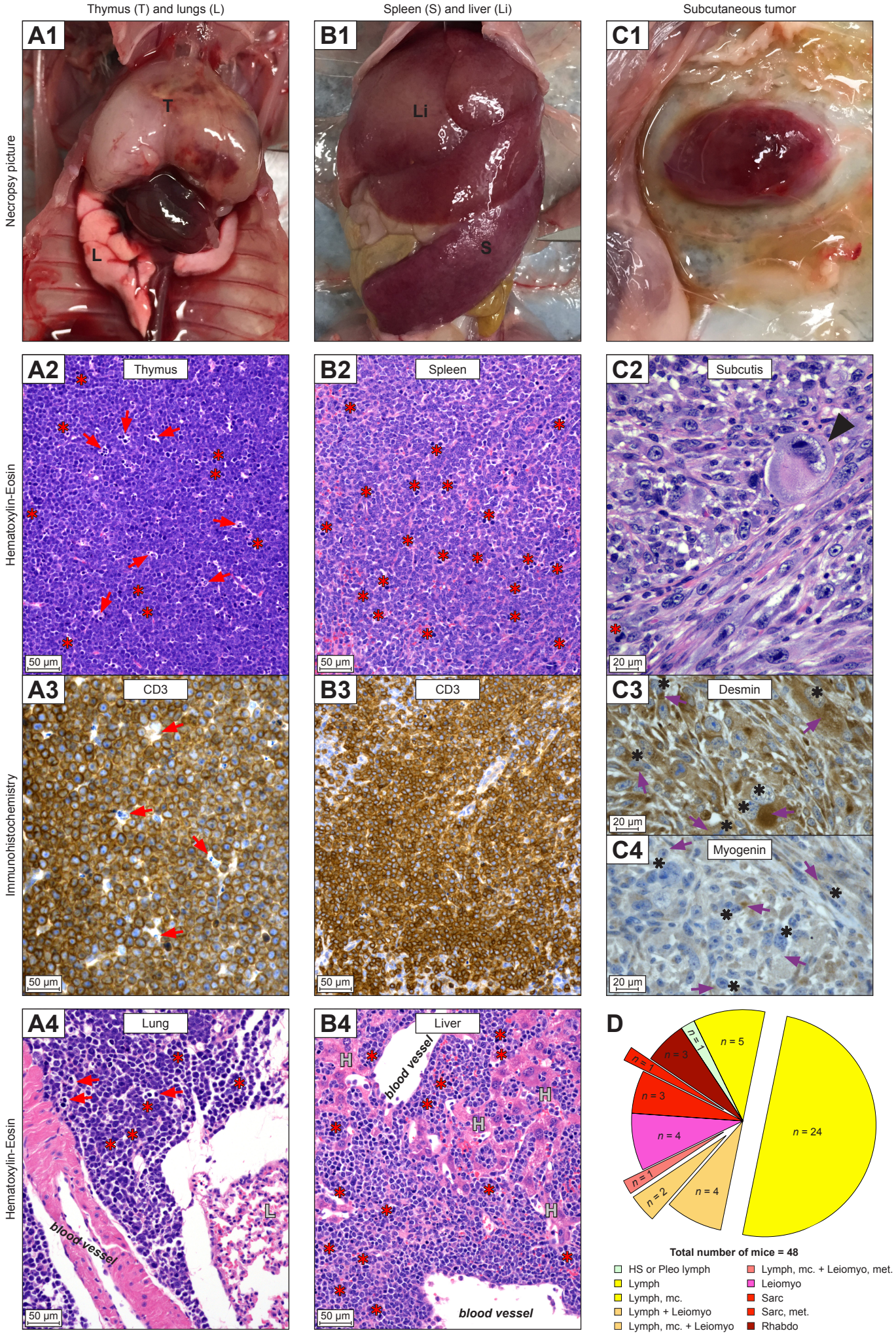
Thymus (T) and lungs (L)
Spleen (S) and liver (Li)
Subcutaneous tumor
Necropsy picture
Hematoxylin-Eosin
Immunohistochemistry
Hematoxylin-Eosin
A1
T
L
B1
Li
S
C1
A2
Thymus
50 µm
B2
Spleen
50 µm
C2
Subcutis
20 µm
A3
CD3
50 µm
B3
CD3
50 µm
C3
Desmin
20 µm
C4
Myogenin
20 µm
A4
Lung
blood vessel
L
50 µm
B4
Liver
blood vessel
H
H
H
H
blood vessel
50 µm
D
n = 5
n = 24
n = 4
n = 4
n = 2
n = 1
n = 3
n = 3
n = 1
n = 1
Total number of mice = 48
HS or Pleo lymph
Lymph
Lymph, mc.
Lymph + Leiomyo
Lymph, mc. + Leiomyo
Lymph, mc. + Leiomyo, met.
Leiomyo
Sarc
Sarc, met.
Rhabdo

Figure 4

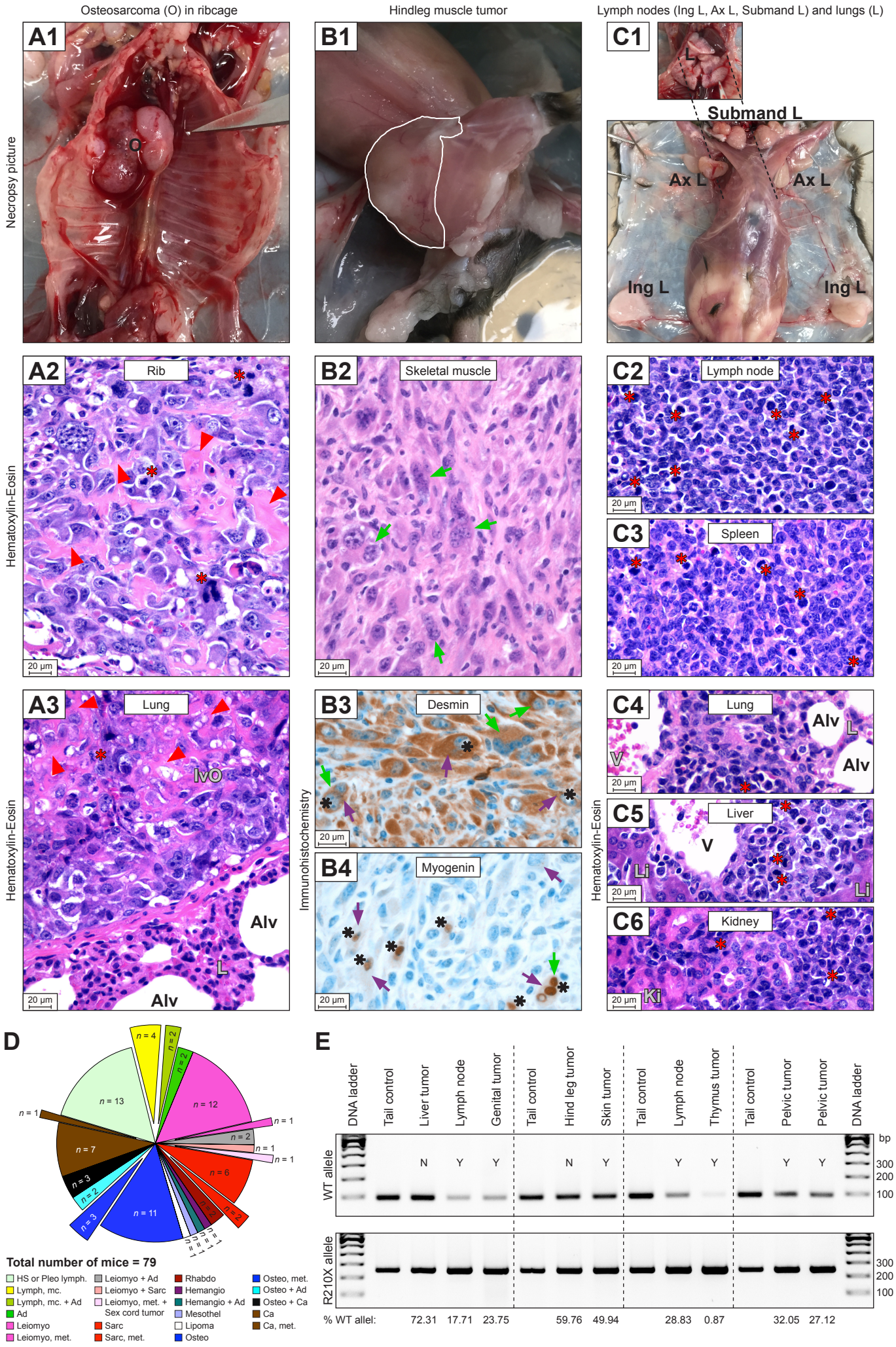
Osteosarcoma (O) in ribcage
Hindleg muscle tumor
Lymph nodes (Ing L, Ax L, Submand L) and lungs (L)
Necropsy picture
Hematoxylin-Eosin
Immunohistochemistry
A1
O
B1
C1
L
Submand L
Ax L
Ax L
Ing L
Ing L
A2
Rib
B2
Skeletal muscle
C2
Lymph node
C3
Spleen
20 µm
A3
Lung
IvO
Alv
L
Alv
B3
Desmin
B4
Myogenin
C4
Lung
Alv
L
Alv
V
C5
Liver
V
Li
Li
C6
Kidney
Ki
D
n = 4
n = 2
n = 2
n = 12
n = 1
n = 2
n = 1
n = 1
n = 6
n = 2
n = 11
n = 3
n = 2
n = 3
n = 7
n = 1
n = 13
Total number of mice = 79
HS or Pleo lymph.
Lymph, mc.
Lymph, mc. + Ad
Ad
Leiomyo
Leiomyo, met.
Leiomyo + Ad
Leiomyo + Sarc
Leiomyo, met. + Sex cord tumor
Sarc
Sarc, met.
Rhabdo
Hemangio
Hemangio + Ad
Mesothel
Lipoma
Osteo
Osteo, met.
Osteo + Ad
Osteo + Ca
Ca
Ca, met.
E
DNA ladder
Tail control
Liver tumor
Lymph node
Genital tumor
Tail control
Hind leg tumor
Skin tumor
Tail control
Lymph node
Thymus tumor
Tail control
Pelvic tumor
Pelvic tumor
DNA ladder
bp
WT allele
N
Y
Y
N
Y
Y
Y
Y
Y
300
200
100
R210X allele
300
200
100
% WT allel:
72.31
17.71
23.75
59.76
49.94
28.83
0.87
32.05
27.12

Figure 5

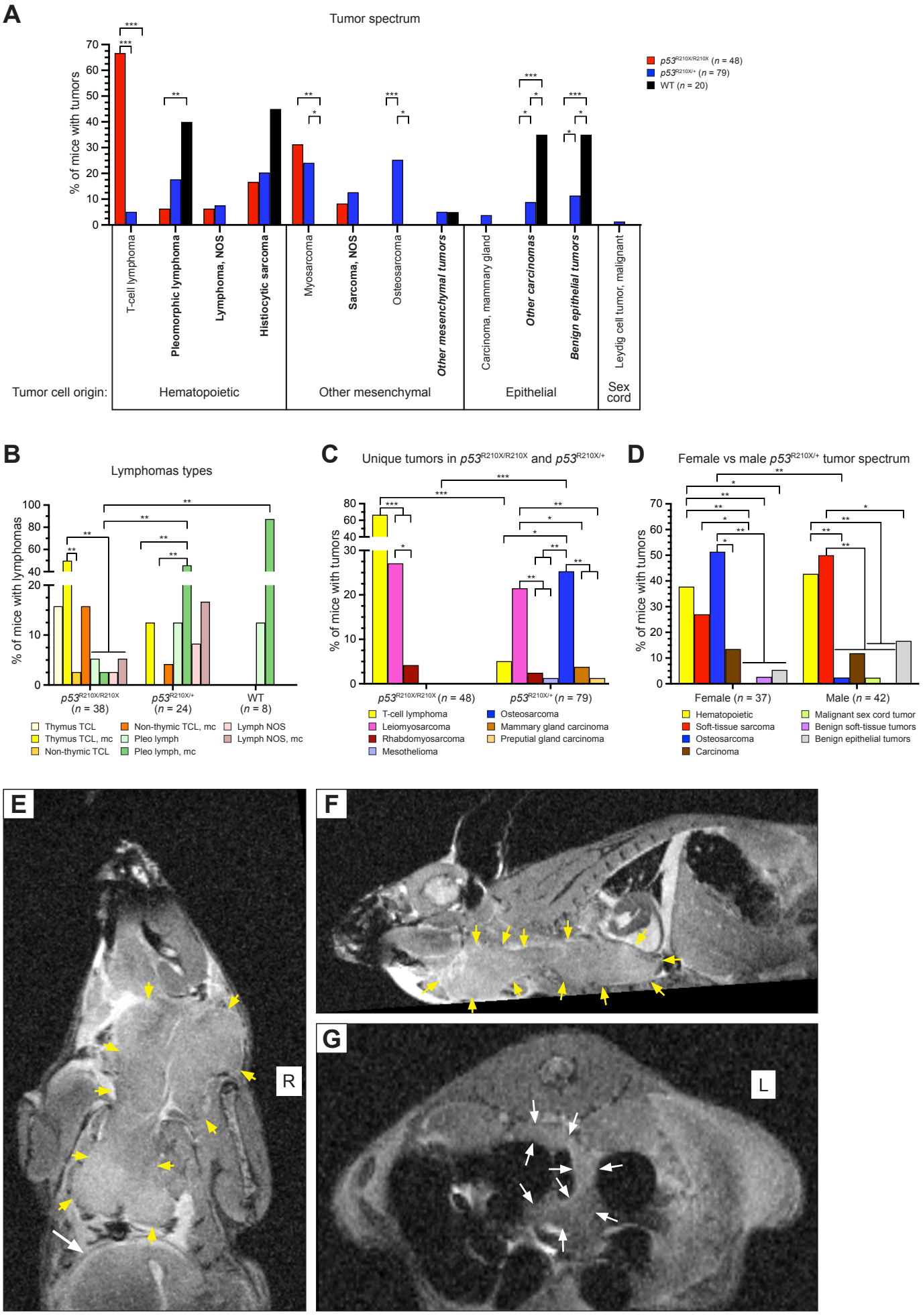
A
Tumor spectrum
% of mice with tumors
p53R210X/R210X (n = 48)
p53R210X/+ (n = 79)
WT (n = 20)
T-cell lymphoma
Pleomorphic lymphoma
Lymphoma, NOS
Histiocytic sarcoma
Myosarcoma
Sarcoma, NOS
Osteosarcoma
Other mesenchymal tumors
Carcinoma, mammary gland
Other carcinomas
Benign epithelial tumors
Leydig cell tumor, malignant
Tumor cell origin:
Hematopoietic
Other mesenchymal
Epithelial
Sex cord
B
Lymphomas types
% of mice with lymphomas
p53R210X/R210X (n = 38)
p53R210X/+ (n = 24)
WT (n = 8)
Thymus TCL
Thymus TCL, mc
Non-thymic TCL
Non-thymic TCL, mc
Pleo lymph
Pleo lymph, mc
Lymph NOS
Lymph NOS, mc
C
Unique tumors in p53R210X/R210X and p53R210X/+
% of mice with tumors
p53R210X/R210X (n = 48)
p53R210X/+ (n = 79)
T-cell lymphoma
Leiomyosarcoma
Rhabdomyosarcoma
Mesothelioma
Osteosarcoma
Mammary gland carcinoma
Preputial gland carcinoma
D
Female vs male p53R210X/+ tumor spectrum
% of mice with tumors
Female (n = 37)
Male (n = 42)
Hematopoietic
Soft-tissue sarcoma
Osteosarcoma
Carcinoma
Malignant sex cord tumor
Benign soft-tissue tumors
Benign epithelial tumors
E
R
F
G
L

Figure 6

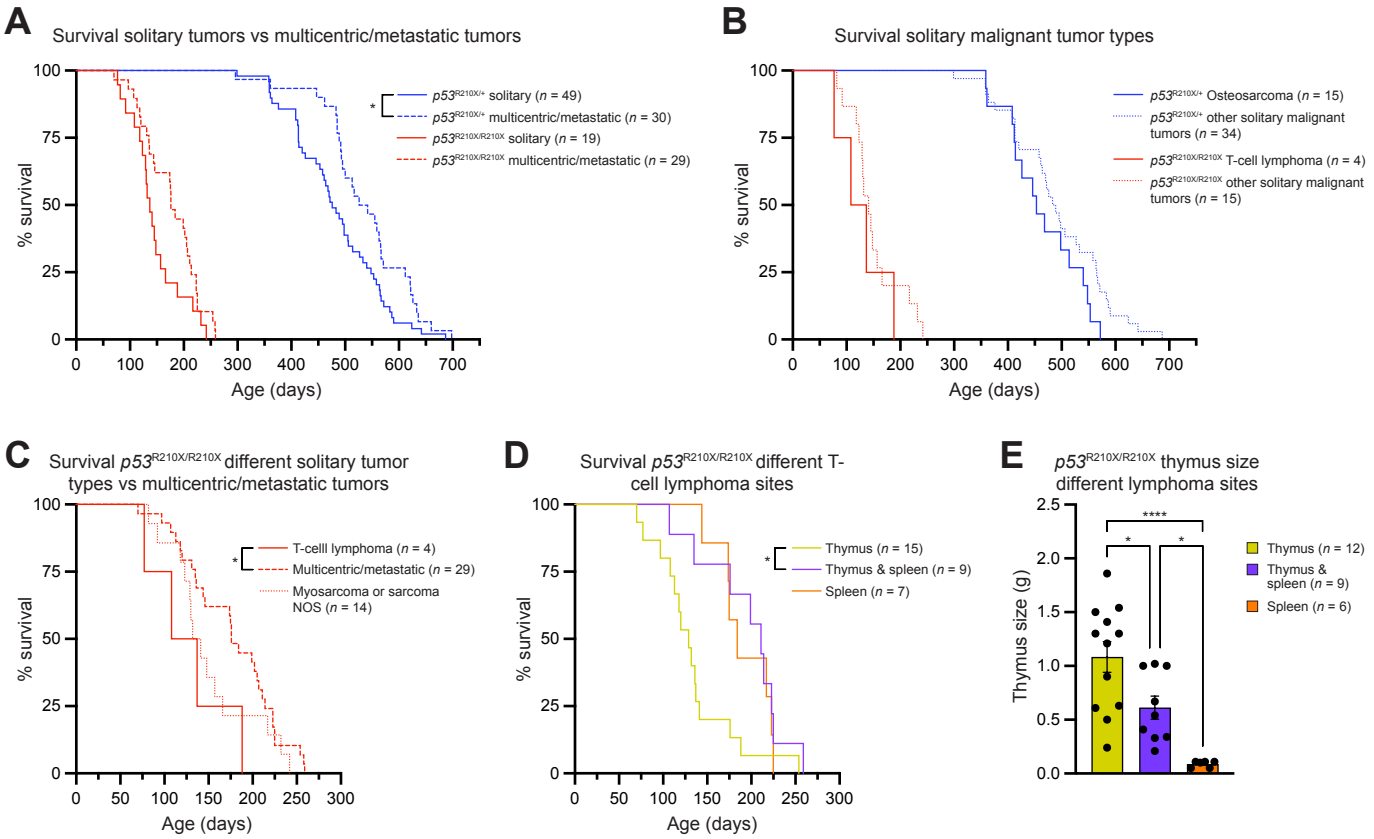
A
Survival solitary tumors vs multicentric/metastatic tumors
% survival
Age (days)
*
p53R210X/+ solitary (n = 49)
p53R210X/+ multicentric/metastatic (n = 30)
p53R210X/R210X solitary (n = 19)
p53R210X/R210X multicentric/metastatic (n = 29)
B
Survival solitary malignant tumor types
% survival
Age (days)
p53R210X/+ Osteosarcoma (n = 15)
p53R210X/+ other solitary malignant tumors (n = 34)
p53R210X/R210X T-cell lymphoma (n = 4)
p53R210X/R210X other solitary malignant tumors (n = 15)
C
Survival p53R210X/R210X different solitary tumor types vs multicentric/metastatic tumors
% survival
Age (days)
*
T-celll lymphoma (n = 4)
Multicentric/metastatic (n = 29)
Myosarcoma or sarcoma NOS (n = 14)
D
Survival p53R210X/R210X different T-cell lymphoma sites
% survival
Age (days)
*
Thymus (n = 15)
Thymus & spleen (n = 9)
Spleen (n = 7)
E
p53R210X/R210X thymus size different lymphoma sites
Thymus size (g)
****
*
*
Thymus (n = 12)
Thymus & spleen (n = 9)
Spleen (n = 6)

Figure 7

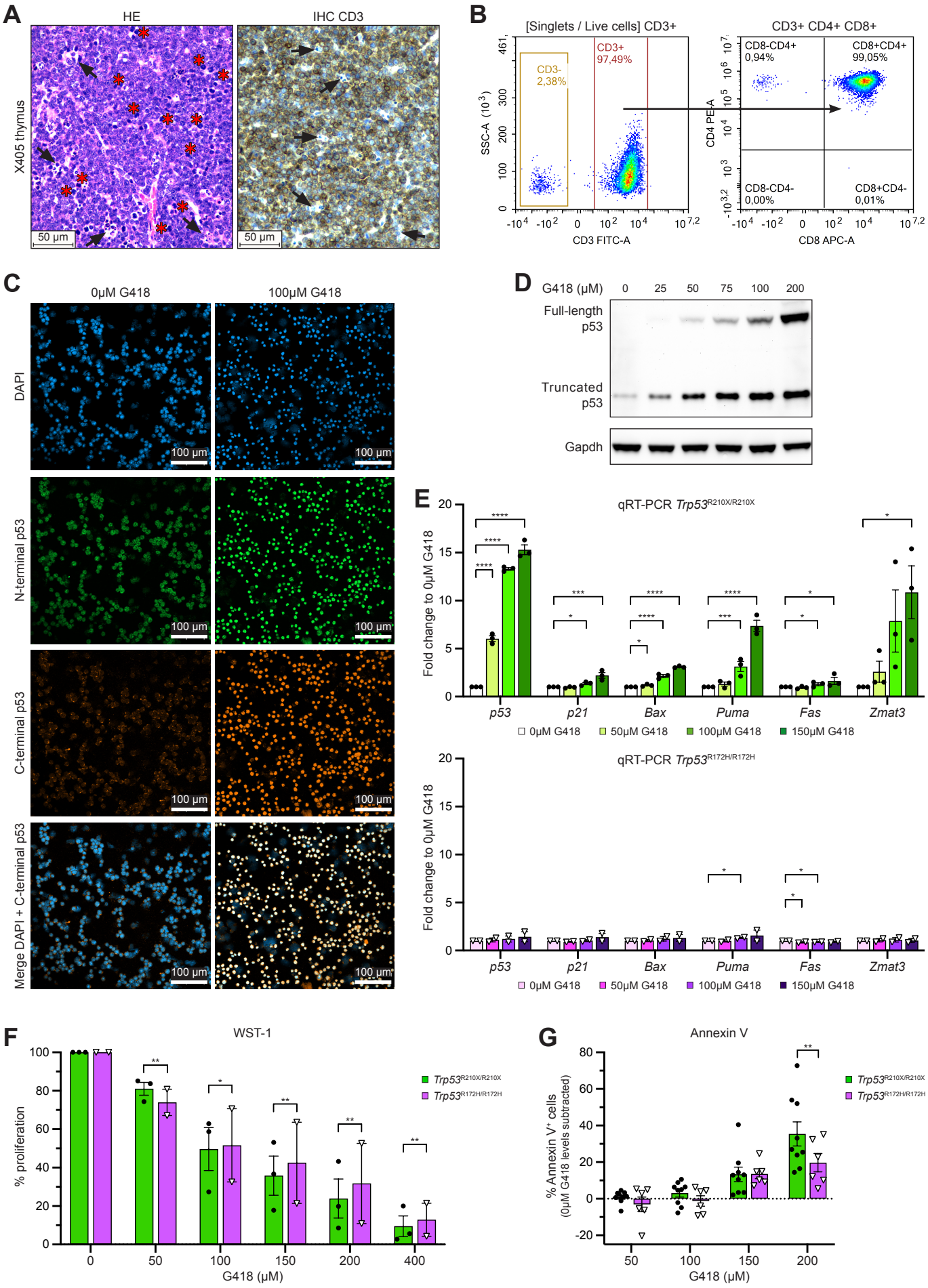
A
HE
IHC CD3
X405 thymus
50 µm
B
[Singlets / Live cells] CD3+
CD3+ CD4+ CD8+
CD3-
2,38%
CD3+
97,49%
SSC-A (10^3)
CD3 FITC-A
CD8-CD4+
0,94%
CD8+CD4+
99,05%
CD8-CD4-
0,00%
CD8+CD4-
0,01%
CD4 PE-A
CD8 APC-A
C
0µM G418
100µM G418
DAPI
N-terminal p53
C-terminal p53
Merge DAPI + C-terminal p53
100 µm
D
G418 (µM)
0
25
50
75
100
200
Full-length p53
Truncated p53
Gapdh
E
qRT-PCR Trp53R210X/R210X
Fold change to 0µM G418
p53
p21
Bax
Puma
Fas
Zmat3
0µM G418
50µM G418
100µM G418
150µM G418
qRT-PCR Trp53R172H/R172H
F
WST-1
% proliferation
G418 (µM)
Trp53R210X/R210X
Trp53R172H/R172H
G
Annexin V
% Annexin V+ cells
(0µM G418 levels subtracted)
G418 (µM)